LBL-8004

UC-25

c.1

POLING EFFECT ON PIEZOELECTRIC BEHAVIOR OF PZT CERAMICS

Shu-Sheng Chiang
(M.S. thesis)

June 1978

Prepared for the U. S. Department of Energy
under Contract W-7405-ENG-48

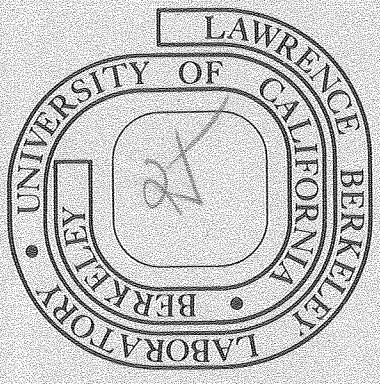

LBL-8004
c.1

POLING EFFECT ON PIEZOELECTRIC BEHAVIOR OF PZT CERAMICS

Shu-Sheng Chiang

Materials and Molecular Research Division, Lawrence Berkeley Laboratory
and Department of Materials Science and Mineral
Engineering, University of California,
Berkeley, California

ABSTRACT

Rod-shaped PZT specimens were sintered with 1 w/o and 5 w/o PbO additives. ZrO_2 segregations were found in the 1% PbO specimen, and higher PbO segregations were found along the grain boundaries and at grain boundary with no ZrO_2 segregations in the 5% PbO specimen. On the basis of these microstructural observations and preliminary poling studies sintered thin disc specimens with a 3 w/o PbO additive were prepared for extensive poling studies.

It was found that the breakdown limit of a specimen depends strongly on the porosity and the pore distribution. The best specimen (3 w/o PbO could be poled at a field of 6kV/mm, a temperature of 100°C and a time of 10 minutes without breakdown. The planar coupling coefficient, K_p, under these conditions was immediately after poling equal to 0.62. This value is the highest among the reported K_p values for pure PZT.

Within the breakdown limit, K_p increases with increase of poling field, temperature and time in a regular manner so that K_p values for other conditions can be predicted. It was found that the specimen became unstable above 125°C even when poled at low fields for short times. It was also found that a high saturated K_p value could not be reached at temperatures below 50°C even when poled for long times.

POLING EFFECT ON PIEZOELECTRIC BEHAVIOR OF PZT CERAMICS

Contents

It was concluded that in general the best conditions for poling are: a temperature as low as possible as long as the temperature is above the critical value at which the K_p of the specimen can reach a high saturated value, a field as high as possible as long as the field does not exceed the breakdown limit, and a time as short as possible as long as K_p reaches the saturated value.

An enhancement of the coupling efficiency was further realized by use of fine rather than coarse PZ+Z packing powder which provided a further control on the rate of loss of PbO from the specimen with a consequent reduction of the porosity of the specimen. This observation emphasizes the importance of controlling the microstructure or character to realize optimum properties.

I. INTRODUCTION

Piezoelectric ceramic materials have been widely used because they are cheap, easy to fabricate compared to single crystals, can survive severe ambient conditions, have the flexibility to be formed into various shapes for specific purposes, and above all, exhibit excellent properties such as extremely large dielectric constants and high coupling coefficients. Among piezoelectric ceramic materials, lead zirconate-titanate (PZT) ceramics have been studied most extensively and are widely used because of their superior properties and versatility over other materials.[1,2] Their dielectric, elastic and piezoelectric properties depend both on composition and processing. The composition effect has been studied extensively by many researchers and results can be found in many references.[3-14] Compared to composition studies, processing variables[15-20] have received less attention and there are many problems left unsolved.

There are two principal steps involved in the processing of piezoelectric ceramic materials. The first step is the fabrication of specimens from raw materials, usually in powder form. The second step is poling which is the application of an electric field across the specimen, usually in thin disc form, to cause the alignment of the randomly oriented domains in the poling field direction, thus increasing the piezoelectric coupling efficiencies.

In this study, problems related to both steps have been studied. The first one was the sintering of a rod-shaped PZT with uniform composition. The second one was a systematic study of the poling effect on the final piezoelectric properties of the material.

A. Sintering a Rod-Shaped Specimen

The advantages of being able to sinter a large specimen include

1) the saving of time, effort and expense during processing, and

2) the availability of a range of shapes for device applications.

High density, large grain size and uniform composition are features that are required to make reliable devices with high piezoelectric coupling efficiencies. High density increases the breakdown strength of the material. Large grain size results in a high coupling efficiency because domains within the grains are easy to reorient without the inhibition of grain boundaries. Uniform composition makes the device reliable and reproducible. Many methods have been used to optimize these characteristics.

Hot pressing[21] can be used to sinter specimens to almost 100% density. Two stage sintering can obtain desired density with controlled grain size.[22] Excess PbO with packing powder, and controlled oxygen atmosphere are used in normal sintering to get dense, stoichiometric specimens.[17,23] Although it is still difficult to control all the parameters at the same time, most of the specimens fabricated by any method can be accepted for certain applications if they are small specimens, namely thin discs, thin plates, etc. The sintering of a large rod-shaped PZT specimen with high density, large grain size and good stoichiometry has not been reported. Normal sintering procedures utilized in making small specimens have not been successful with larger rods. In this study an isostatic pressing step has been used instead of a cold pressing step prior to sintering. Using isostatic pressing, the green density and fired density of the specimens have been increased. Excess PbO is still

needed as it is in normal sintering of thin disc specimens in order to control stoichiometry.

B. Poling

The importance of poling was first recognized by R. B. Gray[24] as reported in his patent. It is considered to be the key step in the development of piezoelectric ceramic materials such as PZT and barium titanate. The first publication of poling effects on barium titanate was by S. Roberts.[25] Since that time, almost all of the piezoelectric specimens obtained after firing were poled to increase the piezoelectric effect of the material. It is now well known that piezoelectric properties of the material vary with field, time, and temperature during and after poling. Increasing the poling field, poling time and poling temperature increases the piezoelectric properties while increasing the time and temperature after poling decreases the piezoelectric properties. Increasing the field after poling increases or decreases the piezoelectric properties depending on the applied field direction to the original poling field direction. A great deal of effort has been made to characterize the behavior of the material after poling because these data are directly used for device applications.[26-34] On the other hand, systematic correlations between the field, temperature and time during poling and the final properties of the material have received much less attention. Therefore, the results obtained after poling are not consistent. Most of the results published[35-37] have been based on specimens that have not been poled sufficiently due to not taking into account processing variables. From a systematic study of the poling behavior, the best conditions for sufficient poling can be established.

Furthermore, the relationships between piezoelectric coupling efficiency and poling condition can lead to a better understanding of the domain switching mechanism during poling.

Nagata studied the field and time effect during poling on lead titanate (PT) ceramics.[38] The results show that the coupling coefficients reach different saturation values under different poling fields if poling time and temperature are sufficiently large. However, Nagata did not systematically study the temperature effect. On the other hand, Takahashi's[39] results, Fig. 1, show that simple relationships between coupling coefficients, field, and time do not exist for PZT ceramics. The coupling coefficient reaches a maximum value at a certain field and time and then decreases when both time and field increase at a constant temperature. This result, although reproduced by Takahashi, can not be explained by the physical mechanism of domain switching during poling. Further experimental work is needed to clarify this result. In this study the poling field, time and temperature were varied systematically to determine the extreme conditions for poling as well as the relationship between poling conditions and coupling coefficients.

II. EXPERIMENTAL

A. Material

Undoped PZT with composition $Pb(Zr_{0.52}Ti_{0.48})O_3$ was selected for this study. No additives were used because the effect of impurities was not a point of consideration. The ratio of Zr/Ti was based on previous studies which indicated that near the morphotropic phase boundary,[40] Fig. 2, PZT achieves maximum coupling efficiency.[1,11] Starting PbO, ZrO_2 and TiO_2 powders were >99.9% pure. Excess PbO was used as a sintering aid. 1 wt% and 5 wt% PbO were used for sintering rod-shaped PZT. 3 wt% PbO was used for sintering thin disc specimens as a comparison.

B. Processing

The processing procedures for preparing both rod-shaped and thin disc-shaped specimens are shown in Fig. 3. The starting oxides, PbO, ZrO_2 and TiO_2, were weighed to form one mole of the indicated PZT. Then the oxides were milled in a vibratory mill for 4 hrs with ZrO_2 balls as grinding media and isopropyl alcohol as lubricant. After mixing, the powder was dried in an oven at 150°C, crushed and isostatically pressed into a slug at 20,000 psi. This step was taken to reduce the PbO loss during calcining. The slugs were calcined at 850°C for 4 hrs in a covered zirconia crucible. X-ray diffraction analysis showed that the solid-state reaction was complete leaving no detectable amount of PbO, ZrO_2 or TiO_2. After calcining, the slugs were crushed while contained in a plastic bag to pass through an 80 mesh screen. This powder was then milled with an excess amount of PbO, polyvinyl alcohol (PVA) which served as a binder for cold pressing, isopropyl alcohol and distilled water. 0.005g PVA was added per gram PZT. The PVA was added as a 4 wt% PVA

solution and diluted about 20 to 30 times in distilled water in order to prevent the PVA from precipitating in the isopropyl alcohol. After 4 hrs of milling, the slurry was dried on a heating plate at 60°C with magnetic stirring during drying. A low temperature was used to prevent PVA evaporation, and magnetic stirring was used to maintain homogeneous mixing. The dried powder was ground and sifted through a 100 mesh screen. Up to this step, the processing was the same for both the rod-shaped and disc-shaped specimens. Beyond this point, the procedures were modified. A half mole of the powder used for the rod-shaped specimen was isostatically pressed at 20,000 psi in a plastic bag with a diameter ≈ 4cm and length ≈ 10cm. The specimen was then covered with lead zirconate (PZ) packing powder in a closed alumina crucible covered with and sintered at 1200°C for 8 hrs in one atmosphere of oxygen. The processing procedure for the preparation of PZ packing powder is shown in Fig. 4. After sintering, the slugs were sliced into pieces 1mm thick and lightly polished to remove the visible scratches made by the diamond saw. Specimens 1.59cm (5/8 inches) in diameter were drilled from the center portion of each piece by an ultrasonic impact grinder. The specimens were electroded by Ag evaporation on both large surfaces before poling.

The rest of the powder was used to make the thin disc specimens. Discs were formed by uniaxially cold pressing 4 to 5 gm of powder at 3,000 psi in a steel die with a 2.54cm, inner diameter. The thickness was approximately 3.2mm. The discs were placed in a high density alumina boat and covered with packing powder. The boat was covered by an alumina plate. Two kinds of packing powder, and PZ + 5 wt% ZrO_2 were used. After sintering at 1200°C for 8 hrs, the specimens were ground to 1mm thickness

by 240 grit and 600 grit SiC. Electrodes were applied on the large surfaces as described before.

C. Materials Characterization

After calcination, specimens were analyzed by x-ray diffraction. After firing, density was determined by the water displacement method. An optical microscope and a scanning-electron microscope were used to analyze the shape and structures of pores, grains and domains. Electron dispersive analysis of x-rays (EDAX) and x-ray mappings attached to SEM were used to detect the presence of any second phase. Electron probe microanalysis (EPMA) was also performed for compositional analyses.

D. Poling

Samples to be poled were ground down to 1 ± 0.01mm thickness. The capacitance and dissipation factor at 1KHz was measured before and after poling using a General Radio Corporation type 1650-A impedance bridge. The poling circuit is shown in Fig. 5. The samples were poled in Dow Corning 704 silicone oil. The temperature was varied from 25 to 150°C. The field was varied from 1kV/mm to 6kV/mm. The time was varied from 1 min to 30 min. The voltage was raised at a constant rate of approximately 100V/sec. The field was removed at the same rate. The resonance and antiresonance frequency of the specimen were measured within 1 hr after poling. Coupling coefficients were calculated according to the 1961 IRE standard. The formulas used during the experiment areas follow.

1) Density measurement

$$D_s = D_{Ni} \frac{W_s}{W_{Ni}} \frac{W_{Ni}-W_{Ni}}{W_s-W_s'}$$

D_{Ni} = density of the nickel standard, 8.90

D_s = sample apparant density

D_s = sample apparant density

W_s = wt. of sample in air

$W_{s'}$ = wt. of sample in distilled water

W_{Ni} = wt. of nickel standard in air

W'_{Ni} = wt. of nickel standard in distilled water

2) Average grain size measurement[41]

$$\text{Average grain size} = \frac{L}{NM}\ (1.5)$$

L = length of the test line on micrograph

N = number of grain boundary intercepts

M = magnification of the micrograph

3) Planar coupling coefficient measurement

$$\frac{k_p^2}{1-k_p^2} = \frac{\left(1-\sigma^E\right) J_1\left[\eta_1\left(1+\Delta f/f_s\right)\right] - \eta_1\left(1+\Delta f/f_s\right) J_o\left[\eta_1\left(1+\Delta f/f_s\right)\right]}{\left(1+\sigma^E\right) J_1\left[\eta_1\left(1+\Delta f/f_s\right)\right]}$$

k_p = planar coupling coefficient

J_o = Bessel function of the first kind and zero order

J_1 = Bessel function of the first kind and first order

η_1 = lowest possible root of $\left(1+\sigma^E\right) J_1(\eta) = \eta J_o(\eta)$

$f_s \approx f_r$ = resonance frequency, $f_p \approx f_a$ antiresonancy frequency,

$\Delta f = f_a - f_r$

The simplified formula for the above expression was given by Dr. Onoe.[43]

$$\frac{1}{k_p^2} = 0.395 \frac{f_r}{f_a - f_r} + 0.574.$$

Both equations have been used to calculate k_p, and they are in good agreement with each other.

III. RESULTS AND DISCUSSION

A. Sintering

I. Rod-Shaped Specimens

On slicing thin disc specimens from the sintered rod specimens, both with 1% and 5% excess PbO, it was observed that the outside part of the rod specimen was dark brown. The color of the inner portion for the 1% PbO specimen was light brown and for the 5% PbO specimen, reddish brown. By optical microscopy the dark colored region was seen to be dense while the inner light colored region was porous. Figure 6 shows this effect for the 1% PbO specimen. Figure 7 shows the same effect for the 5% PbO specimen but the density of the inner portion is higher than that for the 1% PbO specimen and agglomeration of pores is indicated. As seen in Table 1, the density of the inner region of 1% PbO was 7.91 (98.9%) and the corresponding density for 5% PbO was 8.03. Since the theoretical density for this composition is 8.00, these data suggest that the 1% PbO specimen is porous and PbO has been lost while the 5% PbO specimen is oversaturated with PbO.

Scanning-electron micrographs of the inner region of the 1% PbO specimen, Fig. 8, show both porosity and a number of black spots segregated either at the junction of grain boundaries or within the grains. EDAX indicates that these black spots are essentially Zr (Fig. 9). Figure 10 is an x-ray mapping of both the inside and outside regions for this specimen. It shows a uniform concentration in the outer region but nonuniform in the inner region. Electron probe microanalysis data (Figs. 11 and 12) support these analyses. The concentration in the outside dark region fluctuates about 2 atomic % (Fig. 11) but appears to be uniform

macroscopically while the concentration in the inside region fluctuates considerably (Fig. 12). All these observations and data indicate that the specimen is porous and nonhomogeneous. Figure 13 shows the domain patterns that exist in the central region of the 1% PbO rod-shaped PZT specimen. Presence of PbO is also noted along grain boundaries and triple points.

Many pores appeared after etching the 5% PbO specimen, Fig. 14b. Scanning electron micrographs at the same magnification (Fig. 14a) of the unetched specimen suggest the presence of second phase regions along the grain boundaries. These regions correspond to the porous regions seen in the etched specimen and were shown by EDAX (Fig. 15) to have a high lead concentration compared to the lead concentration in the normal grains. This evidence indicates that excess PbO, which was added to introduce a liquid phase during sintering, was not removed completely from the specimen during sintering. The presence of this PbO accounts for the bulk density of the specimen being above 8.00.

The dark region of higher density around the rim of both the 1% and 5% PbO rod-shaped specimens can be explained by a pressure gradient formed in the compacted green bodies prior to sintering. During isostatic pressing, the outer regions of the rods experience higher pressures than the inner regions. Therefore, the outside regions have higher green densities than the inside regions. During sintering the outside regions densify first to form a high density structure. The inside regions, with lower green densities, are prevented from densifying by the outside dense regions which have reached their maximum density. The inside structure thus shows many small pores. The reason for forming

spots with inhomogeneous concentration, however, is not clear. It may be due to decomposition of PZT powders during sintering or evaporation of PbO which did not react to form PZT during calcination. It is of interest to note that some of the high zirconia concentration spots have high PbO spots associated with them nearby. Figure 6 shows pores associated with the high zirconium concentration spots. These pores are assumed to have been the PbO-rich regions described previously.

II. Thin Disc Specimens

For comparison with sliced rod-shaped specimens, the first sintered thin disc specimens were sintered with 3% excess PbO using PZ packing powder. The fired bulk densities were equal to the theoretical value of 8.00, Table 1. Nevertheless, traces of PbO showed up in the x-ray diffraction pattern and the structures of the grain boundary junctions (Fig. 16b) suggested the presence of a PbO phase. The amount of PbO in the specimen, however, is negligible compared to the amount of excess PbO existing in the 5% PbO rod-shaped specimens. The specimen showed a uniform average grain size of 4.6μm. No high Zr spots were observed as in the 1% PbO specimen. The composition is generally homogeneous throughout the specimen. The optical micrograph (Fig. 16a), however, shows that agglomeration of pores can be found occasionally inside the specimen.

The second sintered thin disc specimens were prepared with 3% PbO using PZ+Z packing powder. The advantage of using this packing powder over PZ packing powder is that the PbO activity of PZ+Z packing powder is fixed during sintering while the PbO activity of PZ packing powder is not fixed. Since the PbO activities of the specimen and powder will reach equilibrium during sintering, the specimen will lose PbO to the packing

powder, as the PbO activity of the specimen is initially higher than that of the packing powder, and remain in the single phase region after sintering. The fixed PbO activity of the PZ+Z packing powder thus insures the reproducibility of the specimen which is not the case with the use of the PZ packing powder. A comparison of the specimens sintered using PZ and PZ+Z packing powders indicated that the latter had a slightly higher fired bulk density (8.01), a more uniform pore distribution (Fig. 17a), smaller grain size (3.5μm), and larger amounts of PbO phase along the grain boundaries. In general, the densities for both sets of specimens sintered as discs were close or equal to the theoretical value.

III. Comparison of Initial Poling Results

The four types of specimens described above were poled at the same conditions: field = 3 kV/mm, temperature = 100°C, and time = 20 mins in order to determine the type to be evaluated further. The planar coupling coefficient, K_p, values are given in Table 1. The current-voltage characteristics for 3 of the specimens during poling are shown in Fig. 18. It has been reported by Okazaki[22] that large grain size and low porosity favor coupling efficiency. Webster[44] showed that PbO deficiency in a powder with a starting ratio of Zr/Ti, 52/48, would decrease the coupling efficiency. Microstructural and compositional analyses of the 1% PbO rod-shaped specimen indicate that its density is the lowest, nonstoichiometry is the largest based on evidence of Zr concentration spots, and the grain size is the smallest. Thus, in accordance with the literature statements its coupling coefficient of 0.18 is the lowest even with an elevated poling temperature of 100°C.

Although the density of the 5% PbO rod-shaped specimens is higher than the theoretical value, the specimens have pores and agglomeration of pores inside the specimen as seen in Fig. (7). Some of the excess PbO that was used as a sintering aid remained along the grain boundaries as a second phase. The significant increase in coupling coefficient over the 1% PbO specimen is considered to be due to a greatly reduced porosity and a slightly increased grain size. Although the coupling coefficient K_p in the 5% PbO rod-shaped specimen is greatly improved, its value is still less than that of the 3% PbO thin disc specimens. This difference can be explained on the basis of variations in uniformity, grain size and the amount of the PbO phase along the grain boundaries. Although there is no explanation in the literature on the influence of excess PbO on the coupling coefficient, it is generally believed that the existence of a second phase will adversely affect the electric properties of PZT materials. As for the two sintered thin disc specimens, their coupling coefficients were identical. The first type of the disc specimens may have a larger value because of the larger grain size. The second type may have a larger value because of less porosity. Therefore, the two types showed the same K_p values. For the subsequent poling studies, we chose the second type of specimen because of its better reproducibility.

B. Poling

I. Breakdown Effect

The biggest problem involved in poling the sample is to achieve the maximum coupling efficiency without breaking down the sample. The unpredictability of the breakdown factors is probably the major reason that makes the systematic study of poling either unavailable or inconsistent.

The breakdown effect not only depends on the dielectric strength of the material but also depends on the microstructure, a variable which is often neglected in such studies. From Fig. 19 it is seen that samples poled at a high temperature breakdown even at low fields for short times. This behavior is due to a weakening of the dielectric strength causing the dissipation current to increase exponentially leading to the breakdown. The magnitude of the dissipation current is between 0.4 and 0.5 mA when the breakdown occurs. Besides this effect, breakdowns also occur at low temperatures and high fields. At low temperatures, the current flowing through the sample is far below 0.4 mA. The current sufficient for poling is below 0.15 mA as can be seen in Fig. 20.

When the temperature is equal to or less than 100°C, the sample still breaks down occasionally at medium fields (3kV/mm ~ 4kV/mm). This effect can not be explained purely by the weakening of the dielectric strength. The microstructure plays an important role. Takahashi indicated that the breakdown path seemed to follow the grain boundaries.[39] If there are pores existing in the specimen the breakdown effect is enhanced when the breakdown channel intersects a pore.[45] Experiments support this suggestion. This result can be explained by the fact that the dielectric permittivity and strength of a pore is much lower than that of the ceramic. A series of specimens was examined before electroding in front of an incandescent lamp. Since the samples are translucent, the larger pores in the sample showed up as black spots. Later poling results show that breakdown first occurs in these spots. If large pores exist, specimens are observed to break down into two pieces. The conclusion from such observations is that specimens should be free of pores.

There is another factor that can contribute to the breakdown of a specimen. During grinding specimens to the desired thickness, some materials may be chipped around the edge by the coarse grinding media. With an irregular field distribution already existing around the edge, this chipping can further increase the local field strength causing breakdown to occur faster. If there are pores near the edge, the breakdown occurs even faster. This behavior explains why in early experiments fully electroded specimens always broke down around the edges first. This troublesome effect can be eliminated by reducing the electrode area on the major surface. In this study only two sets of specimens were fully electroded, i.e. samples poled at 100°C, 3kV/mm and 1.8 kV/mm, for different times. The rest of the specimens were all partially electroded. The ratio of the diameters of the electrode area to total area was 0.8. With partially electroded surfaces, it was possible to avoid the troublesome breakdowns that could have occurred around the edges as the poling field was increased from 3kV/mm to 6kV/mm. The only breakdown that was observed occurred at a field of 6.7kV/mm and 100°C near the edge of the partially electroded surface which further supported this interpretation.

In addition to breakdown problems, there is still the question of the proper ratio of the diameter of a partially electroded area (d_p) and the diameter of a fully electroded area (d_f). If the ratio is too small, the coupling result will be underestimated for the partially electroded specimen compared to the result of the fully electroded specimen. Schnabel[46] has demonstrated the effective thickness coupling coefficient (K_t) of partially electroded disc PZT specimens vs. their normalized electrode diameter i.e., d_p/d_f. Since K_t and D_p do not differ much for

our PZT sample, we can assume that the above result also holds for the K_p value. Then the difference in K_p between partially electroded specimens and fully electroded specimens should be very small because the normalized diameter ratio is 0.8. Experiments for specimens poled at 3kV/mm, 20 min., 100°C and 4kV/mm, 1 min, 100°C show that the coupling coefficient K_p is the same for both the partially electroded specimens and fully electroded specimens. This problem apparently did not exist in this study; it should however, be kept in mind. The planar coupling coefficients of specimens used in subsequent poling studies were listed in Table 2.

II. Electric Field Dependence

To study the field dependence, the time was kept constant, the field was varied from 1kV/mm to 6kV/mm and temperatures of 25°C, 50°C and 100°C were used. The results are shown in Fig. 20. It can be seen that when the field increases, K_p increases. However, the behavior at 100°C is different. Replotting the data on a semi-log basis (Fig. 21), it is shown that K_p increases exponentially with field at 25°C and 50°C. At 100°C, K_p increases exponentially at low fields, then increases rapidly and approaches a saturated value. It would appear logical that with further increase in field at 25°C and 50°C the same behavior would be exhibited. The breakdown effect, however, limits the field range. Seven to 8kV/mm is approximately the upper limit for specimens to be poled at 100°C. The exponential increase of coupling coefficient at low temperatures also occurs in PT ceramics even if the coupling coefficient is K_t. Nagata's[28] data for PT ceramics, replotted on a semi-log basis, Fig. 22, showed a straight line at 25°C and K_t saturation values at 100

and 200°C.

It can be concluded that on poling below some critical temperature the coupling coefficient increases exponentially until the poling field reaches the breakdown limit. At this field limit, the coupling coefficient is too low to show a good coupling efficiency. On the other hand, at higher poling temperatures, the coupling coefficient increases rapidly after passing through the initial exponential range and approaches a saturated value.

III. Temperature Dependence

The results shown in Fig. 21 indicate that K_p increases with increasing temperature. To study the temperature dependence of K_p systematically, the poling field was fixed at 3kV/mm. Temperatures were varied from 25°C to 125°C. Times of 5 mins, 10 mins and 20 mins were used. The results, as listed in Table 2, are shown in Fig. 23. Again, replotting the data on a semi-log basis, Fig. 24, it is shown that K_p increases exponentially with temperature until poling temperature is above 100°C. Above 100°C, it approaches a saturation value. This behavior holds for all specimens poled more than 5 mins.

Among all the test specimens shown in Fig. 24, only the result of the specimen poled at 75°C for 5 mins did not fall on the expected straight line which indicates the logarithmic increase of K_p with temperature. The discrepancy may be caused by the following factors: The porosity of the specimen was higher than others, or the temperature of the specimen was not in equilibrium with the temperature of the silicone oil bath during the poling experiment. Both factors lower the coupling coefficient.

To find the maximum temperature suitable for poling, we chose 150°C as a start. Breakdown of the specimen occurred at 3kV/mm. The time elapsed was less than 30 seconds. The current-voltage behavior for the specimen subject to this poling condition is shown in Fig. 25. It indicates the upper current limit of the breakdown effect, as we have described before. The subsequent experiment of poling the specimen at 150°C, 2kV/mm for 1 min showed that 150°C is not a suitable temperature for poling because the coupling coefficient is only 0.38, which is much less than the values obtained for specimen poling at lower temperatures, higher fields for 1 min (see Table 2). The C-V curve for the above poling condition is shown in Fig. 26. When the specimen was poled at 140°C, 4kV/mm, it broke down within 1 min (see Fig. 27). The specimen broke down again at 125°C, 4kV/mm within 4 mins, Fig. 28. If we avoid reaching the breakdown limit by poling the specimen at 3kV/mm for 125°C, the specimen reaches a saturated value of 0.58 for poling time of 20 mins. From the C-V curve, Fig. 29, it is seen that the current already exceeds 0.15mA and the specimen will soon reach the current breakdown within 10 to 15 mins. This temperature is also not suitable for poling. When the temperature was further lowered to 100°C, the breakdown effect occurred at 6.7kV/mm in less than 1 min. However, the specimen can be poled at 6kV/mm for more than 10 mins without breaking down. The coupling coefficient K_p reaches the highest value among the results obtained from all poling conditions in this study. For practical poling purposes, the specimen can be poled at 100°C, 6kV/mm for 5 mins which is still not at the breakdown limit, the K_p obtained can be as high as 0.60. Therefore, it is concluded that 100°C is the most suitable temperature for poling

PZT specimens without additives.

IV. Time Dependence

In this study, the poling temperature was fixed at 100°C. Poling times varied from 1 min to 20 mins or 30 mins. The field was varied from 1.8kV/mm to 6kV/mm for comparison. Results of K_p vs. time are shown in Fig. 30. When the specimen was poled at a low field of 1.8kV/mm, K_p increased slowly with time and reached saturation when it was poled more than 20 mins. Since the slope of the curve, Fig. 30, above 20 mins, is not zero, a slight increase in K_p is expected. However, it is so low that it can not reach the K_p value of specimens poled at high fields. This is due to the fact that a large number of 90 degree domains can not be realigned along the field direction under low field conditions.

As the field is increased to 3kV/mm, K_p increases more rapidly with time and soon reaches a saturation value. The saturation values at different poling fields do not differ much once the field is above 3kV/mm, and the times required for K_p to approach the saturation values become less as the field increases. Since K_p of the specimen poled at 6kV/mm for 1 min has almost the same value as that poled at 4kV/mm for 20 mins, we would certainly choose the poling condition to be 6kV/mm for 1 min due to the fact that time is saved and the dielectric loss of the specimen is reduced.

V. Influence of Packing Powder and Liquid Phase on Coupling Coefficient

From Fig. 30, it can be seen that K_p increases with time rapidly and then reaches a saturation value. However, Takahashi's results indicated that there is a particular poling time and field at which K_p is

maximum (Fig. 1). If the field was kept at 4kV/mm, the maximum K_p occurred when the specimen was poled for 5 mins and then K_p decreased with increased time. If the field was kept at 5kV/mm, all the specimens poled for different times will have lower coupling coefficient K_p compared to K_p of the specimen poled at 4kV/mm for the same time, and K_p increases monotonically as time increases. It appeared that there is a factor offsetting the domain realignment poling at high field or long time under elevated temperatures. This difference must result from the different properties of the specimen. The first difference between our specimens and Takahashi's is that his reported densities are 7.7-7.8 g/cm^3 and ours are $8.00 \pm 0.02\ g/cm^3$. The second difference is that his reported average grain size is 22μm and ours is 3.5μm.

According to Okazaki's result,[22] large grain size should favor the increase of coupling coefficient compared to small grain size under the same poling conditions. But under extreme poling conditions (i.e. temperature 100°C, field $\geq$ 4kV/mm, time $\geq$ 10 mins), this effect seems to be less important compared to the effect of porosity or defect concentration. The effect of low density in his specimen indicates the existence of high porosity or large defect concentrations. Under severe poling conditions, a large space charge field formed due to the existence of pores and defect concentrations. This field, in turn, offsets the original poling field and the coupling coefficient decreases. The processing factors that may cause these differences in properties are most likely to be 1) the addition of a liquid phase, 2) the difference in packing powder.

Excess PbO formed a liquid phase during sintering which not only increases the density but also reduces the loss of PbO from the PZT phase to the packing powder. With the proper amount of liquid phase added, porosity of the specimen can be greatly reduced with an increase in the breakdown field limit and suppression of the space charge field inside the specimen during poling. In their processing, no excess PbO was added and low density is not avoided.

The efficiency of packing powder, used to maintain the PbO activity of the specimen, not only depends on the types of packing powder chosen, but also on the particle size of the packing powder used. In Takahashi's processing, calcined PZT powder was used as packing powder, with the size unspecified. Since PZT is a single phase material, the activity of PbO is not fixed during sintering. Therefore, specimens, as well as packing powder, lose PbO continuously and the reproducibility of the specimens is reduced.

It has also been observed that the efficiency of packing powder depends on its particle size. If the particle size of PZ+Z packing powder is reduced to less than 100 mesh, K_p increases compared to the result using coarse packing powder under the same poling condition (Table 3). The variation of K_p with time using fine packing powder is shown in Fig. 31. It can be seen that K_p increases rapidly and maintains a saturation value without decreasing even when poled for 90 mins. In addition, the increase in K_p does not affect the field dependence of K_p as has been described earlier (Fig. 32).

IV. CONCLUSIONS

Microstructural observations indicated that sintering a rod-shaped specimen with 1% PbO in PZ packing powder caused the appearance of high Zr concentration spots along grain boundaries or inside the grains. This behavior indicates loss of PbO from the specimen. On the other hand, sintering a 5% PbO rod-shaped specimen showed the appearance of high PbO concentration along the grain boundaries as a second phase. The proper amount of excess PbO to be used as a liquid phase sintering aid on the basis of these experiments is thus between 1% and 5% PbO. Thin disc-shaped specimens were then prepared with 3% PbO. It was found that the nature of the packing powder was equally important. Reproducibly dense thin disc specimens were obtained with the use of PZ+Z rather than PZ packing powder. Enhanced poling efficiency was further realized by use of fine rather than coarse powder.

A poling study revealed that within the breakdown limit the planar coupling coefficient or coupling efficiency (K_p) increases with time, field and temperature. Experiments showed that specimens became unstable at high temperature ($\geq$125°C) even at low fields. The best poling temperature was found to be 100°C. At this temperature, specimens could be poled at 6kV/mm for more than 10 mins without breakdown. A coupling coefficient of 0.62 was obtained which is among the highest values reported for PZT compositions without additives. Systematic studies of the poling effect on coupling efficiency showed that Kp increases with field, but these high saturation values were not reached within 20 or 30 mins except at a temperature of about 100°C.

Reproducibility of poling characteristics is dependent upon reproducibility of the character of the specimens. Two specimens poled under the same poling conditions showed different coupling coefficients because of differences in porosity and pore distribution. Porous specimens are subject to easy breakdown on poling. Freedom from pores is then one of the most important characteristics for obtaining high, reproducible coupling efficiencies.

ACKNOWLEDGMENT

I am deeply indebted to the late Professor Richard M. Fulrath who guided me into this field. I am also grateful to Professor Joseph A. Pask and Professor R. H. White for their invaluable council and patience throughout this work, and Professor Alan W. Searcy and R. S. Muller for their enlightening discussions and editing of this thesis.

The help of my fellow graduate students throughout this work is greatly acknowledged. Further thanks are extended to Gay Brazil, Richard Lindberg, Gloria Pelatowski and Jack Wodei for their technical assistance.

Finally I would like to express special thanks to my parents for their continuous encouragement and support.

This work was supported by the Division of Materials Sciences, Office of Basic Energy Sciences, U.S. Department of Energy.

Table 1. Comparison Between the Rod-Shaped and Disc-Shaped Specimens of $Pb(Zr_{0.52}Ti_{0.48})O_3$ Sintered in PZ Packing Powder

Shape	Excess (PbO)	Packing Powder	Density (g/cm^3)	Grain Size (μm)	Planar Coupling Coefficient, K_p
rod	1 w/o	PZ	7.91*	3.1	0.18
rod	5 w/o	PZ	8.03*	3.7	0.49
disc	3 w/o	PZ	8.00	4.6	0.54
disc	3 w/o	PZ+Z	8.00	3.5	0.54

*Inner region of rod-shaped specimens.

Table 2. Poling Results of 3% PbO Disc-Shaped Specimens Sintered in Coarse PZ+Z Packing Powder

Temperature (°C°)	Field (kV/mm)	Time (min)	Surface Electroded Area or (Full or Partial)	Planar Coupling Coefficient
150	3	1	P	0.55
	2	1	P	0.38
140	4	1	P	0.56
125	4	4	P	0.50
	3	20	P	0.56
	3	10	P	0.57
	3	5	P	0.55
100	6	10	P	0.62
	6	5	P	0.60
	6	1	P	0.59
	5	30	P	0.61
		10	P	0.59
		5	P	0.59
		1	P	0.54
	4	20	P	0.60
		10	P	0.58
	4	5	P	0.56
	4	1	P	0.41
	3	20	F	0.54
		10	F	0.49
		5	F	0.44
		1	F	0.29
	1.8	20	F	0.28
		10	F	0.27
		5	F	0.16
	1	5	P	0.11
75	3	20	P	0.31
		10	P	0.28
		5	P	0.17
50	6	5	P	0.32
	4	5	P	0.24
	3	20	P	0.18
	3	10	P	0.16
	3	5	P	0.13
	1	5	P	0.07
25	6	5	P	0.22
	6	5	P	0.23
	4	5	P	0.12
	3	5	P	0.097
	3	20	P	0.105
	3	10	P	0.083
10	7	5	P	0.28

Table 3. Poling Results of 3% PbO Disc-Shaped Specimens Sintered in Fine PZ+Z Packing Powder

Temperature (°C)	Field (kV/mm)	Time (min)	Planar Coupling Coefficient (K_p)
100	1.8	5	0.19
		20	0.28
		60	0.35
	3	5	0.51
		20	0.60
		30	0.60
		60	0.61
		90	0.62
		240	0.61
	4	5	0.62
	5	5	0.65
	6	5	0.66

FIGURE CAPTIONS

Fig. 1. Variation in the planar coupling coefficient K_p with time in $Pb(Zr_{52}Ti_{48})O_3$ as determined by Takahashi.[39]

Fig. 2. PZT phase diagram.

Fig. 3. Processing flow chart for PZT specimens.

Fig. 4. Processing flow chart for packing powder.

Fig. 5. Poling circuit.

Fig. 6. Microstructure of PZT + 1% PbO rod-shaped specimen:

(a) Difference in density between inner (bottom) and outer (top) regions of the sample.

(b) Inner region microstructure showing both pores and segregation spots.

(c) High magnification photo of outer region.

(d) High magnification of inner region.

Fig. 7. Optical micrograph of PZT + 5 w/o PbO rod-shaped specimen.

(a) 80X

(b) 400X

(c) 400X

Illustrating a pore agglomerated region.

Fig. 8. SEM of PZT + 1 w/o PbO rod-shaped specimen.

(a) Outer region

(b) Inner region showing segregation spots.

Fig. 9. Composition identification in 1 w/o PbO rod-shaped specimen by EDAX.

(a) Segregation spots showing high Zr concentration.

(b) Composition in normal grain region. Order of peaks is Zr, Pb and Ti.

Fig. 10. X-ray mapping photos for 1 w/o PbO rod-shaped specimen
(a) Pb, (b) Zr, (c) Ti, and (d) Pb.
a, b, and c were taken from a section in the inner region, and d from the outer region.

Fig. 11. Concentration profile through a section from the outer region of the 1 w/o PbO rod-shaped specimen by electron probe microanalysis.

Fig. 12. Concentration profile through a section from the inner region of the 1 w/o PbO rod-shaped specimen by electron probe microanalysis.

Fig. 13. SEM of selected region in 1 w/o PbO rod-shaped specimen showing patterns of 90° and 180° domains. Second phase of PbO also noted along grain boundaries and triple points.

Fig. 14. Microstructure of 5 w/o PbO rod-shaped specimen.
(a) Unetched, (b) etched
Whitish regions in (a) becoming pores in (b) due to second phase.

Fig. 15. Composition identification in 5 w/o PbO rod-shaped specimen by EDAX:
(a) White portions show high Pb concentration.
(b) Composition in normal grain region. Order of peaks is Zr, Pb and Ti.

Fig. 16. 3 w/o PbO disc-shaped specimen sintered in PZ packing powder.
(a) Optical micrograph illustrating the pore distribution and agglomeration.
(b) SEM illustrating the microstructure.

Fig. 17. 3 w/o PbO disc-shaped specimen sintered in PZ+Z packing powder.
(a) Optical micrograph illustrating uniform structure with almost no pores.
(b) SEM illustrating the uniformity of the microstructure and lesser amount of PbO second phase.

Fig. 18. Current-voltage characteristics of three types of specimens during poling as recorded by X-Y plotter for indicated conditions.

Fig. 19. Current-voltage behavior for the 3 w/o PbO thin disc specimen showing breakdown behavior for poling condition of 150°C and 3kV/mm.

Fig. 20. Current-voltage characteristics of 3 w/o PbO disc-shaped specimen sintered in PZ+Z packing powder during poling as recorded by X-Y plotter for indicated conditions.

Fig. 21. Variation of planar coupling coefficient with poling field for indicated conditions for 3 w/o PbO disc-shaped specimen sintered in PZ+Z packing powder.

Fig. 22. Replot of Fig. 21 on semi-log basis.

Fig. 23. Nagata's results[38] of the variation of thickness coupling coefficient of PT specimen with poling field.

Fig. 24. Variation of planar coupling coefficient K_p of 3 w/o PbO disc-shaped specimen with poling temperature.

Fig. 25. Replot of Fig. 24 on semi-log basis.

Fig. 26. Current-voltage behavior for 3 w/o PbO disc specimen for given poling conditions.

Fig. 27. Current-voltage behavior for 3 w/o PbO disc specimen for given poling conditions.

Fig. 28. Current-voltage behavior for 3 w/o PbO disc specimen for given poling conditions.

Fig. 29. Current-voltage behavior for 3 w/o PbO disc specimen for given poling conditions.

Fig. 30. Variations of planar coupling coefficient K_p with poling time for 3 w/o PbO disc specimen sintered in PZ+Z packing powder.

Fig. 31. Same as Fig. 30 except that the specimen was sintered in finer particle size of PZ+Z packing powder.

Fig. 32. Comparison of K_p vs. poling field for 3 w/o PbO disc-shaped specimens sintered in fine (white circle) and coarse (black circle) PZ+Z packing powder.

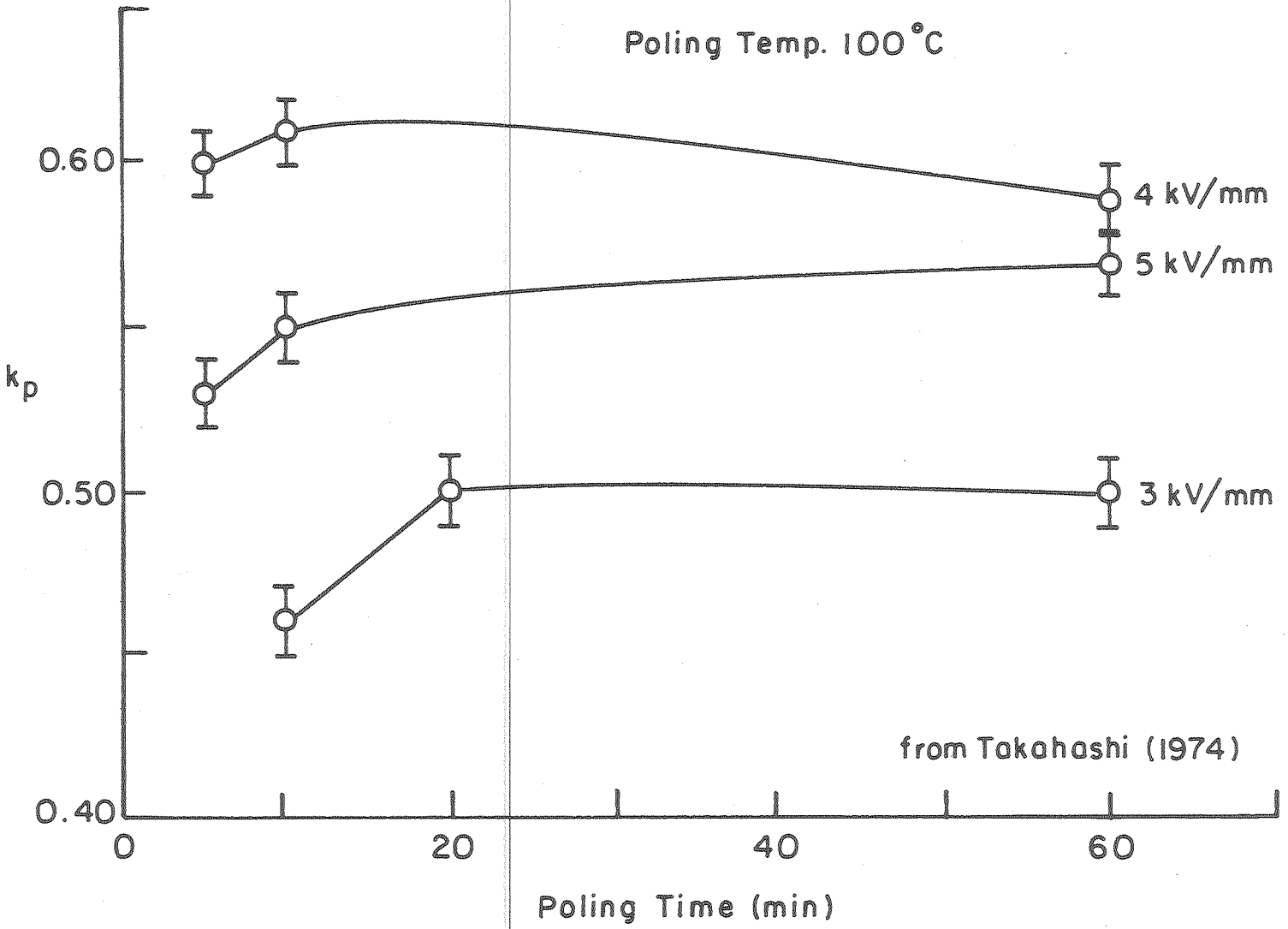

XBL 784-4894

Fig. 1

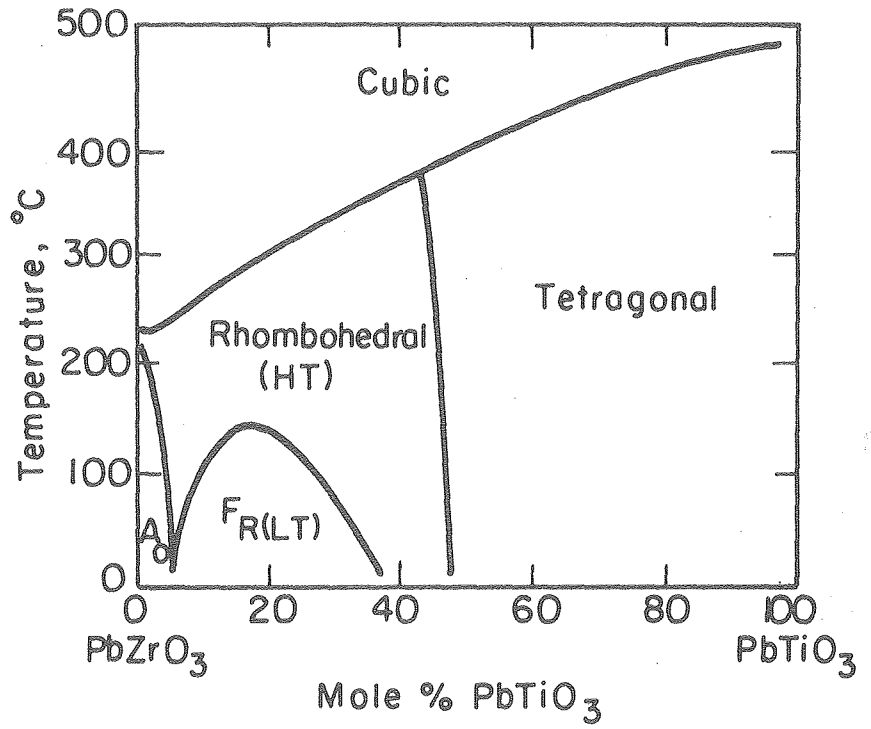

The $PbZrO_3$ - $PbTiO_3$ phase diagram.

Fig. 2

PROCESSING DIAGRAM FOR PZT POWDER

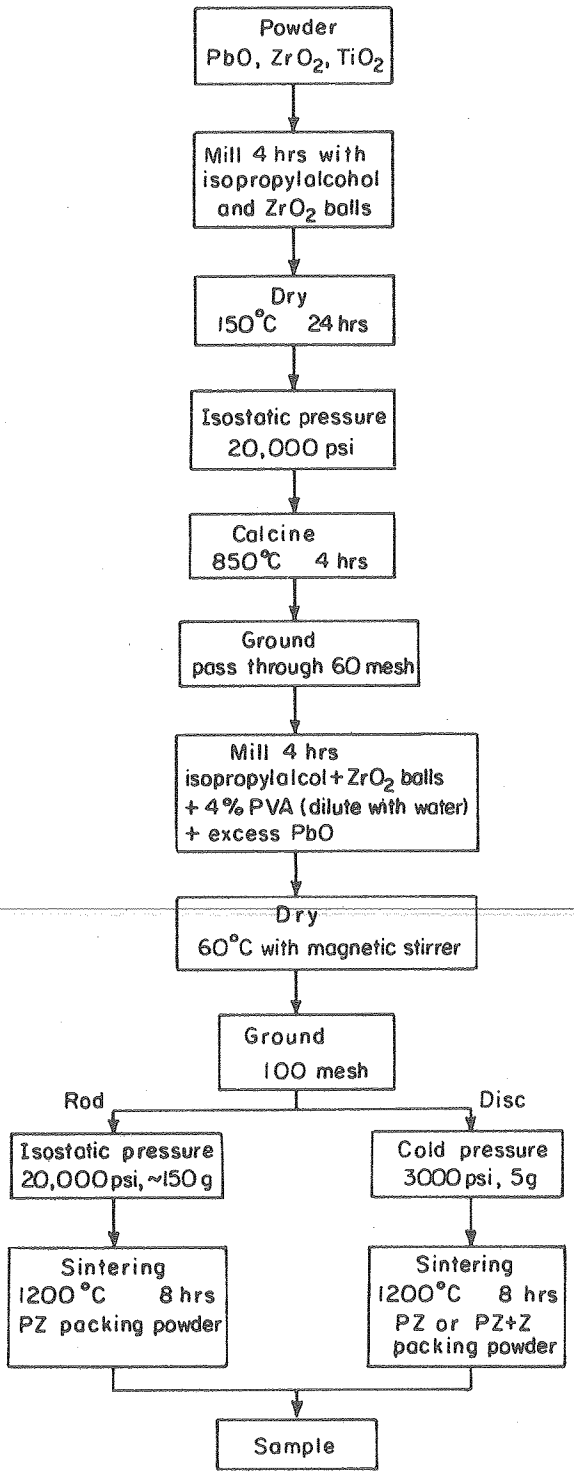

XBL 784-4901

Fig. 3

PROCESSING DIAGRAM FOR PZ OR PZ+Z
PACKING POWDER

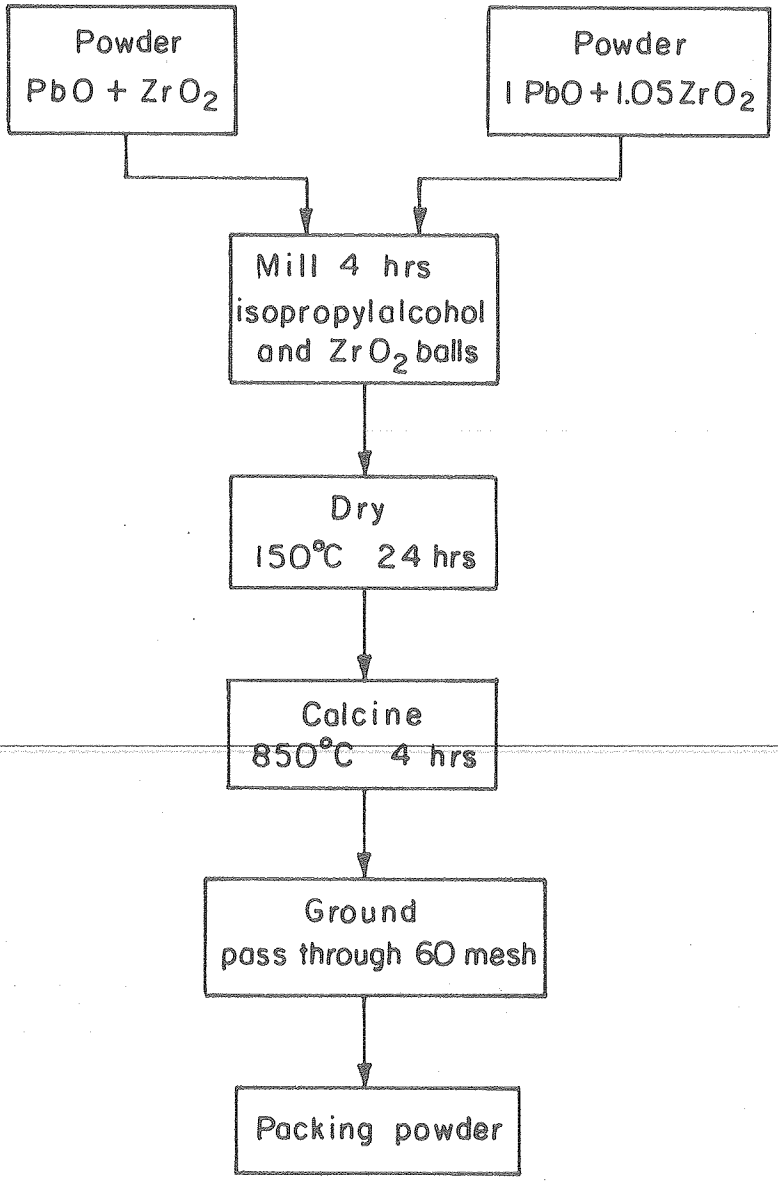

XBL784-4902

Fig. 4

POLING CIRCUIT

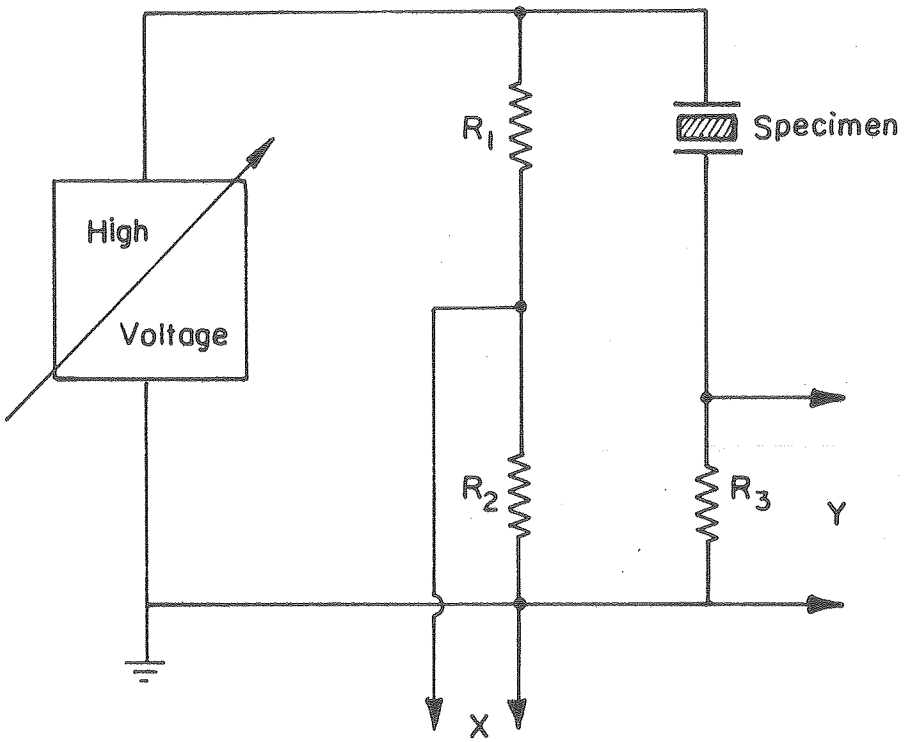

R_1 = 51.1 MΩ

R_2 = 1 kΩ

R_3 = 10 kΩ

On the X-Y Plotter:

X axis — Voltage drop across specimen

Y axis — Current through specimen

XBL784-4903

Fig. 5

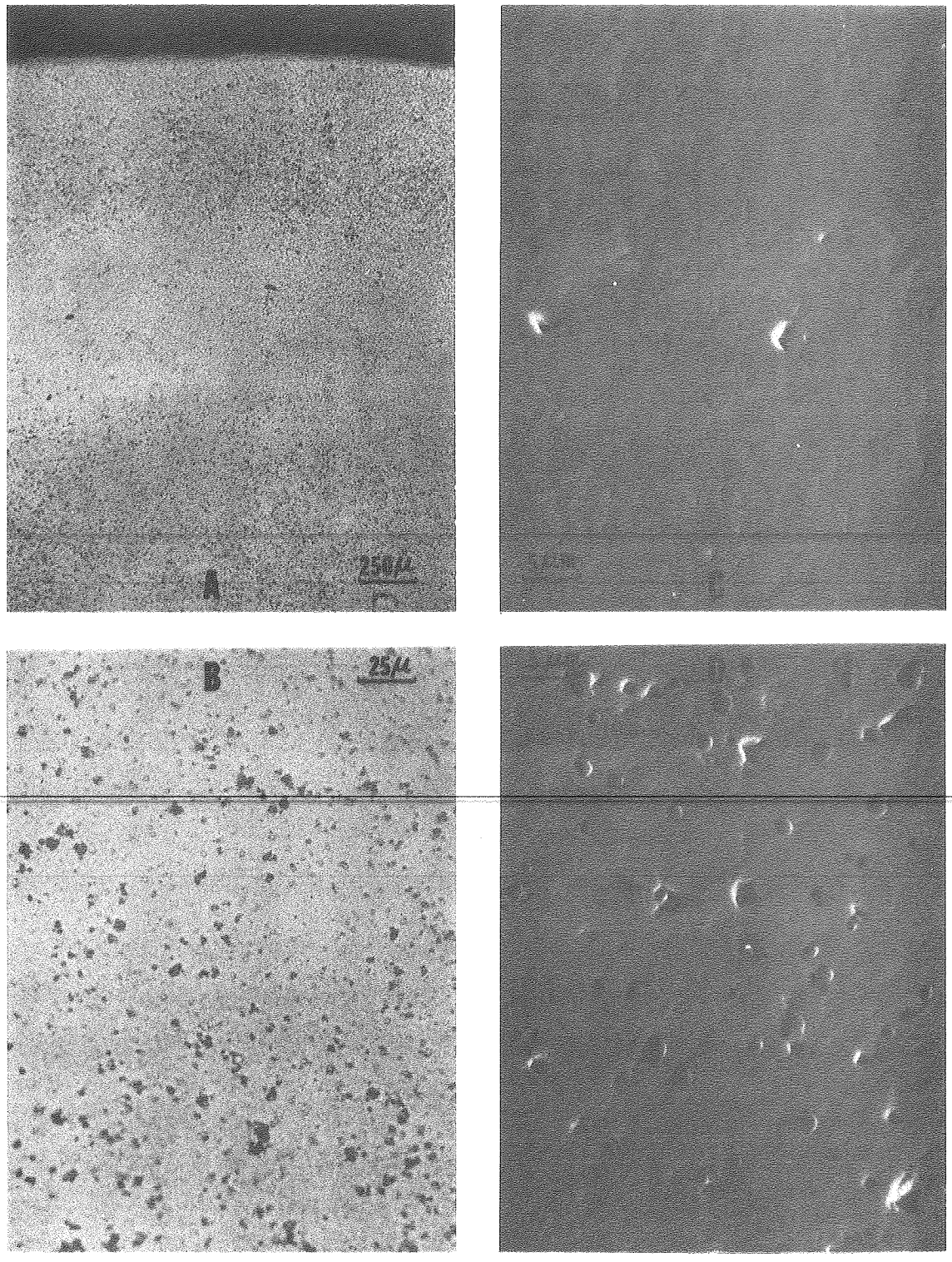

XBB785-5122

Fig. 6

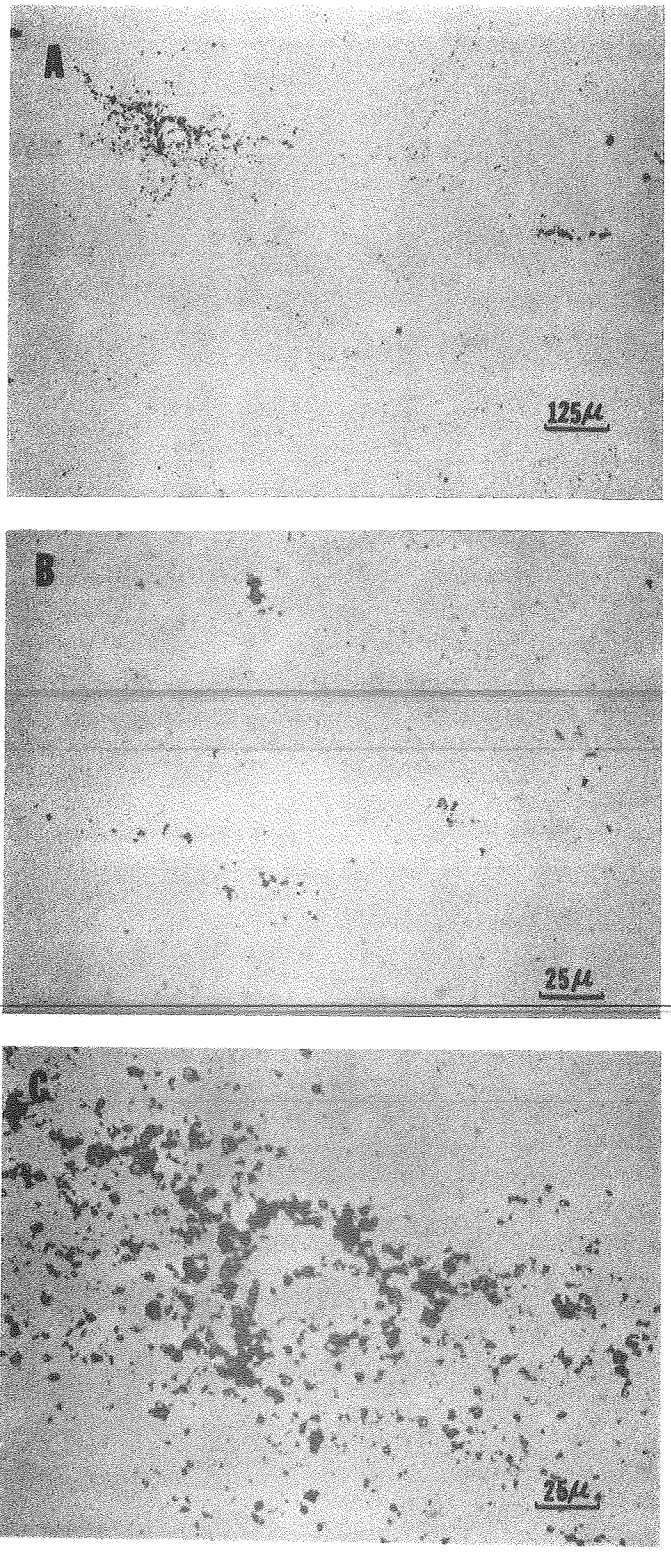

XBB785-512

Fig. 7

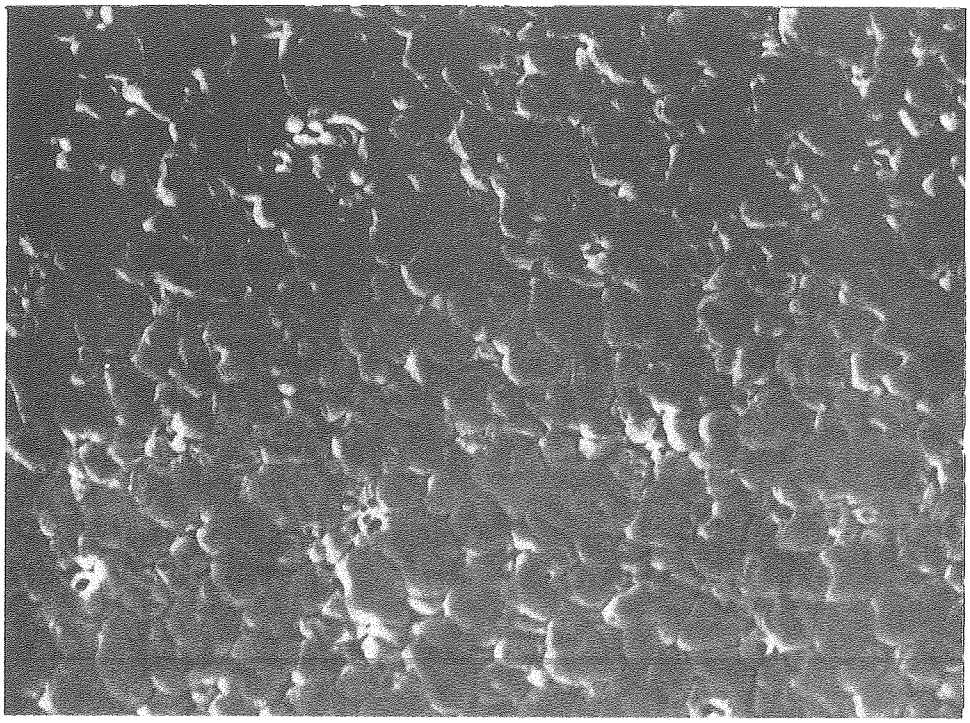

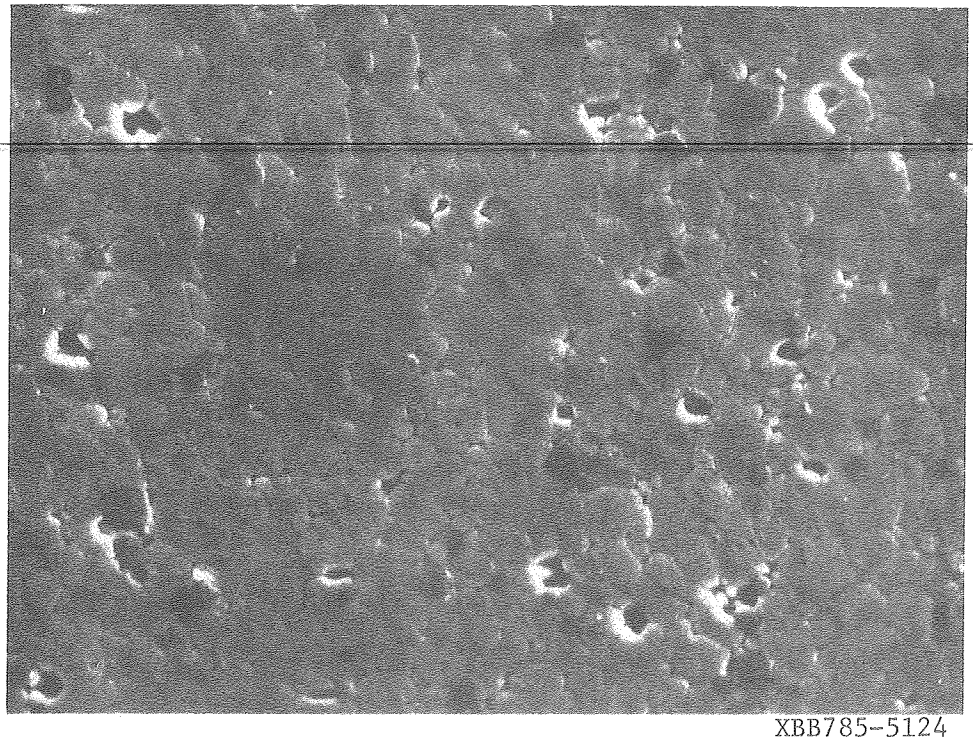

XBB785-5124

Fig. 8

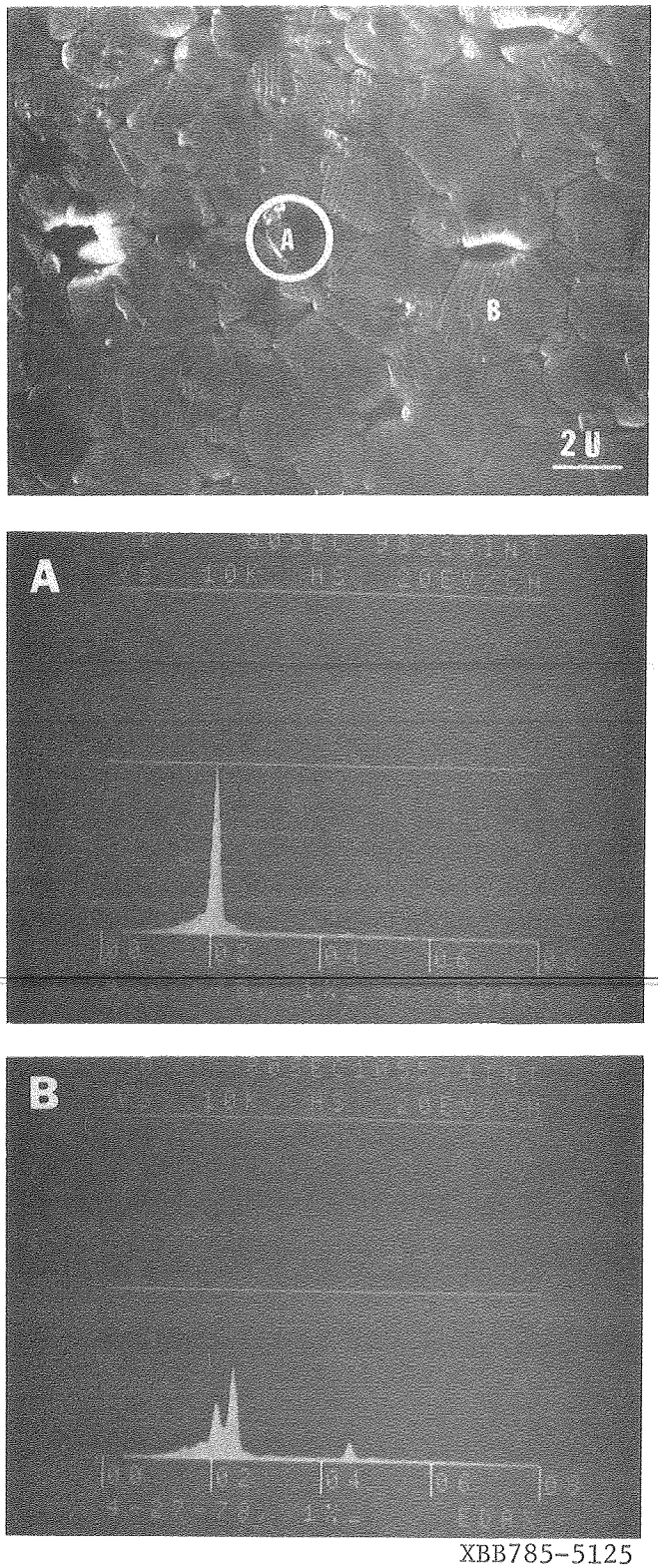

XBB785-5125

Fig. 9

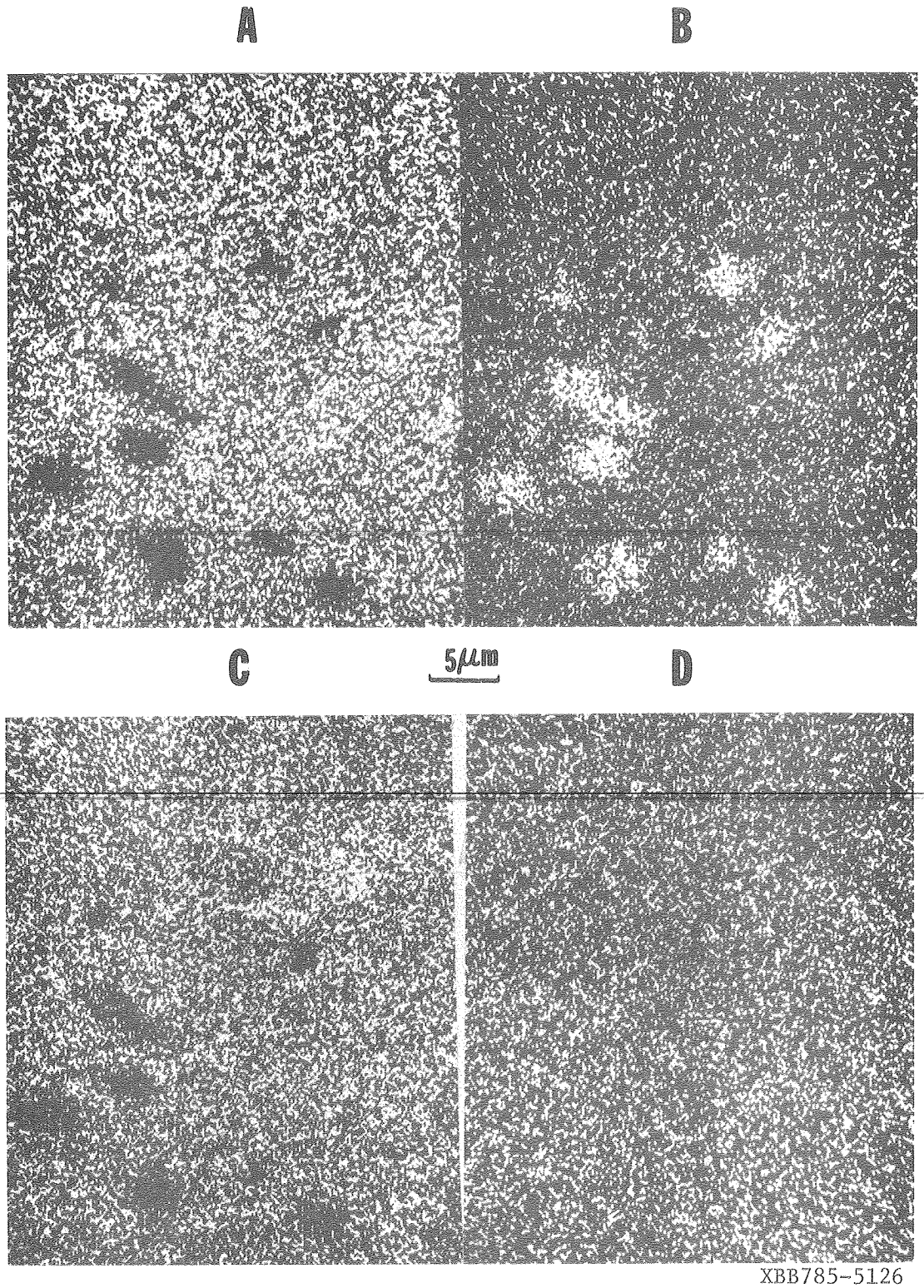

XBB785-5126

Fig. 10

XBL 784-4893

Fig. 11

1 W% PbO Rod Shape Sample
(inner region)
Concentration
Pb
Zr
Ti
Atomic Concentration (At %)
Distance in Microns (μ)
XBL784-4892

Fig. 12

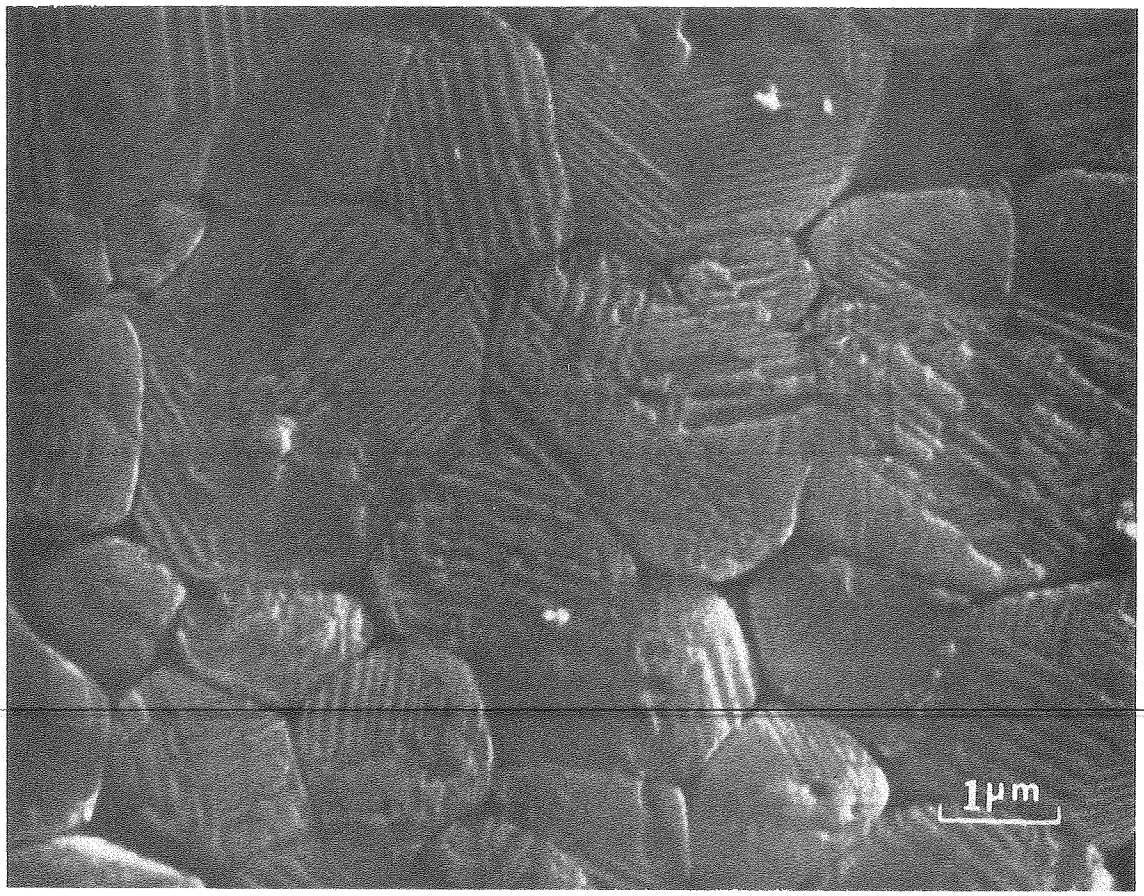

XBB785-5127

Fig. 13

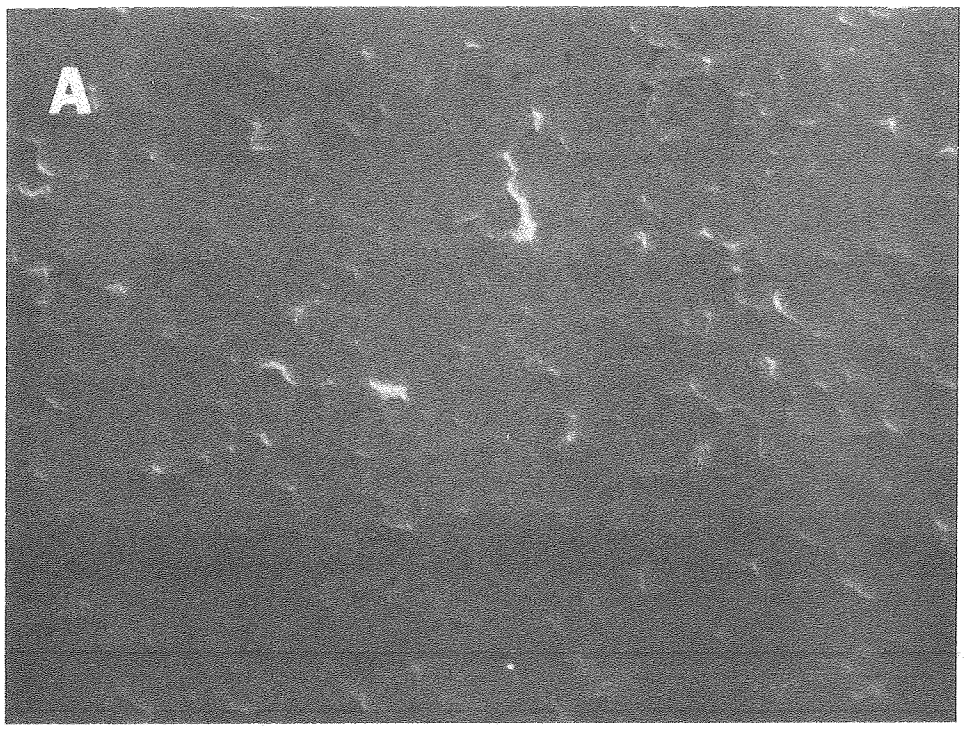

5μm

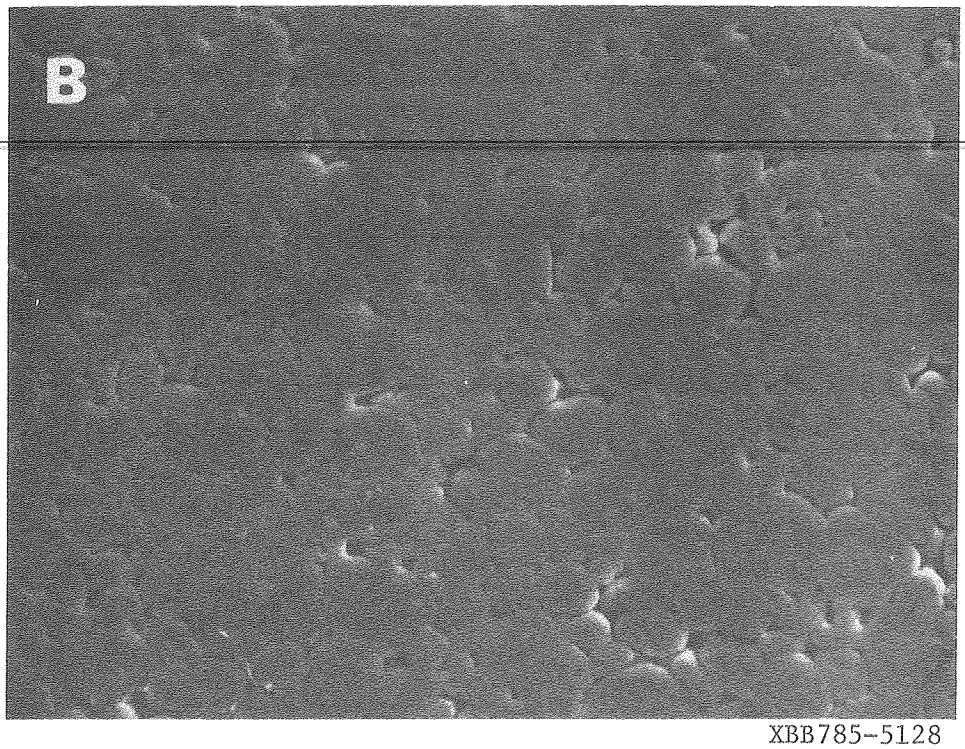

XBB785-5128

Fig. 14

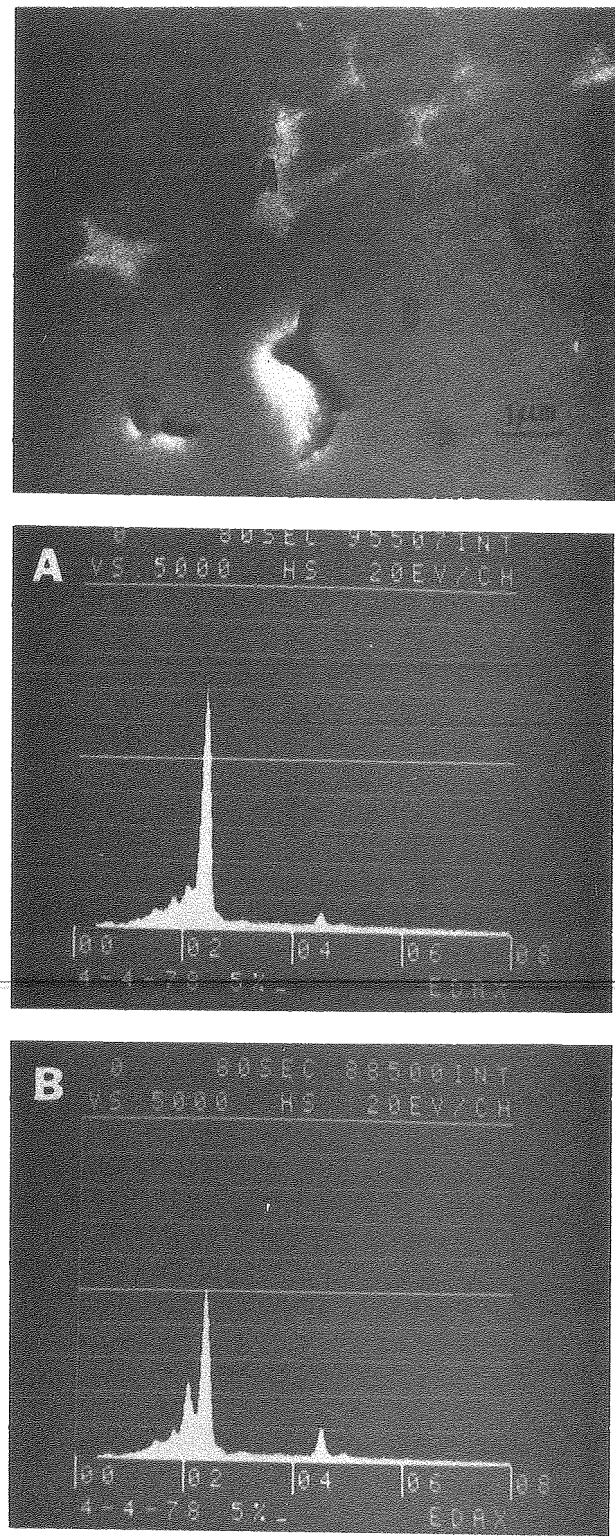

XBB785-5129

Fig. 15

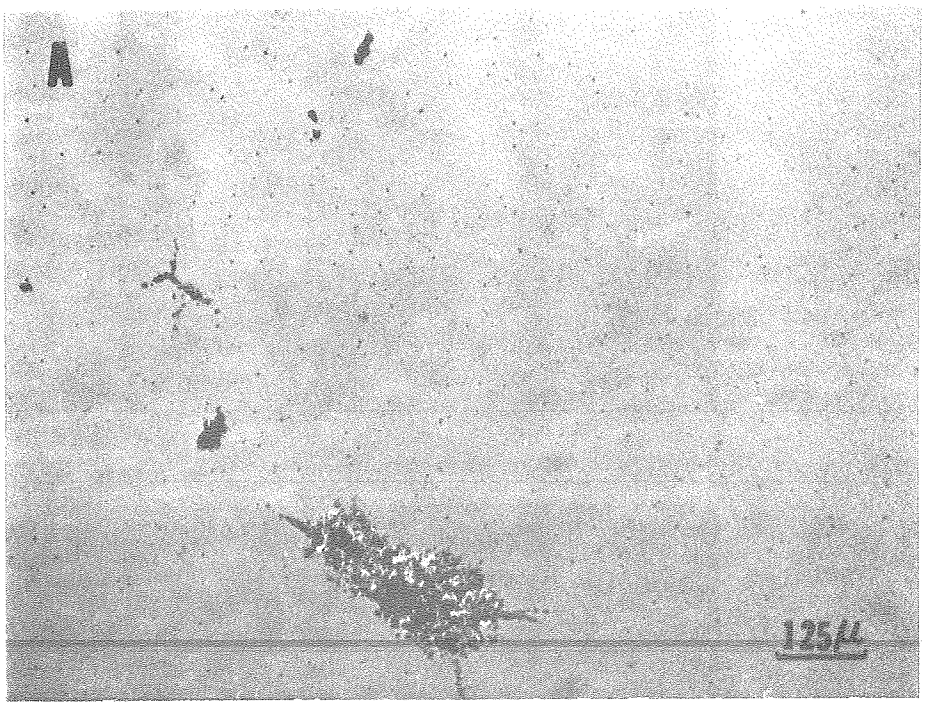

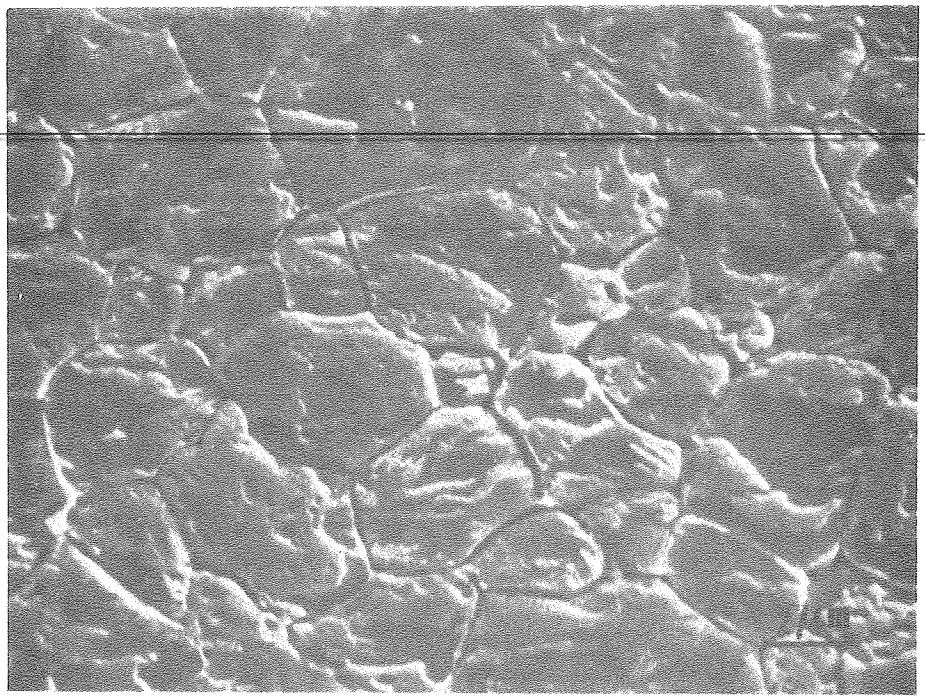

XBB785-5130

Fig. 16

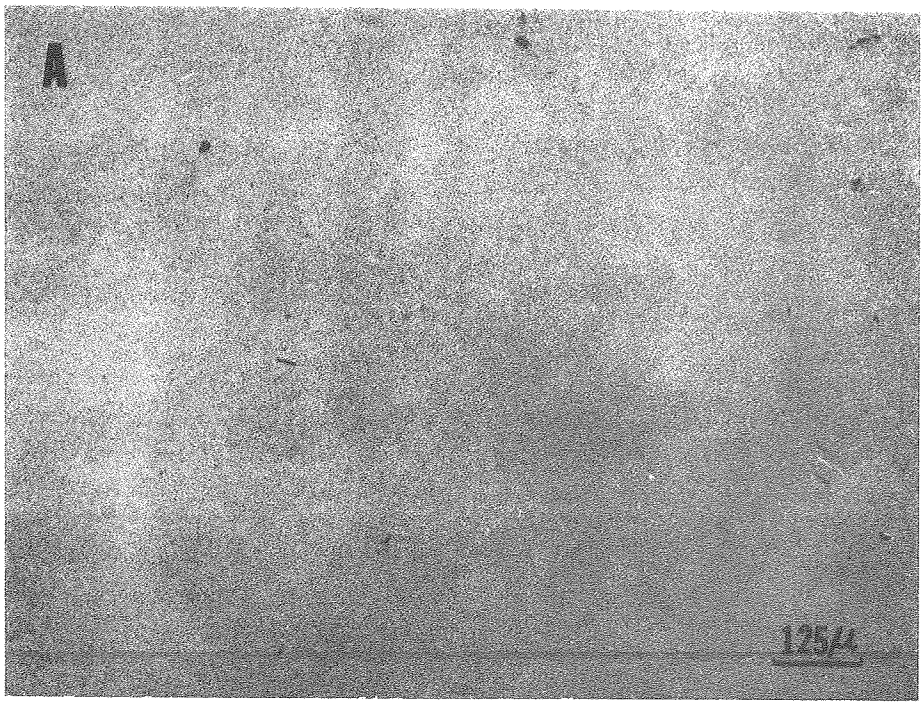

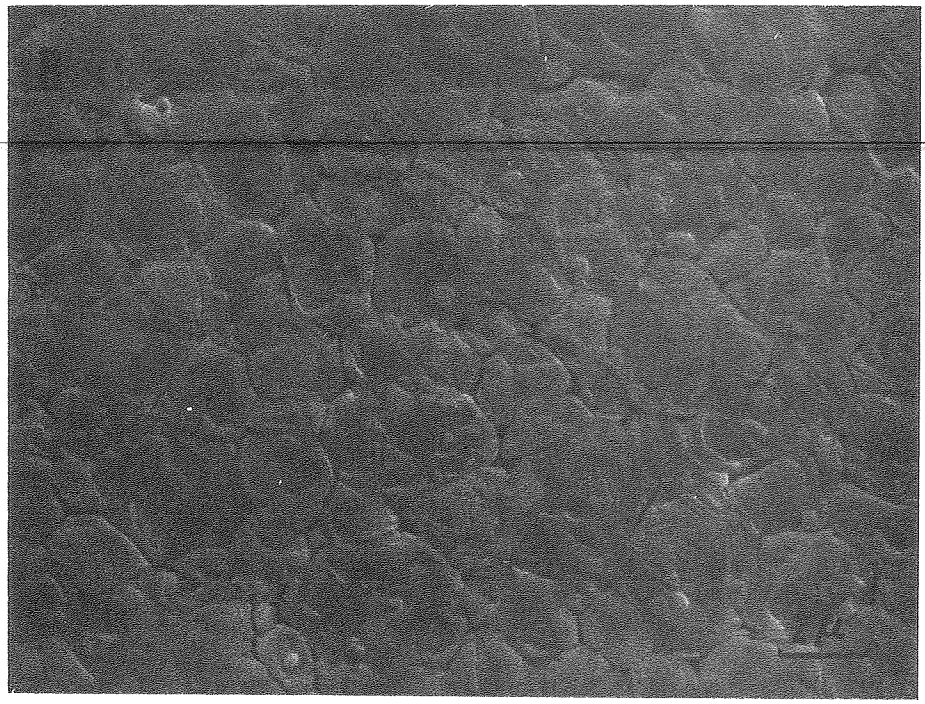

XBB785-5131

Fig. 17

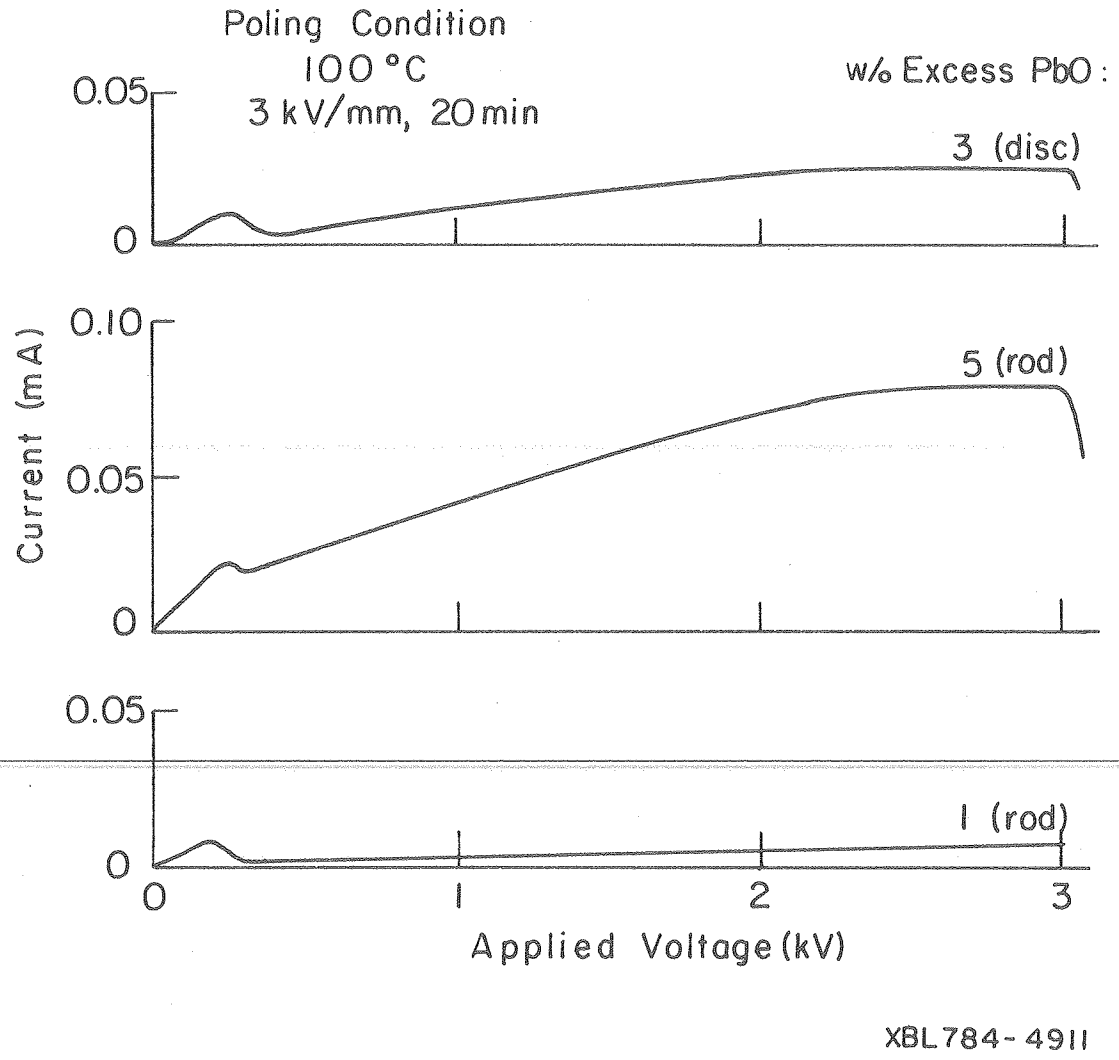
Poling Condition
100 °C
3 kV/mm, 20 min
w/o Excess PbO :
0.05
0
3 (disc)
0.10
0.05
0
5 (rod)
Current (mA)
0.05
0
1 (rod)
0
1
2
3
Applied Voltage (kV)
XBL784-4911

Fig. 18

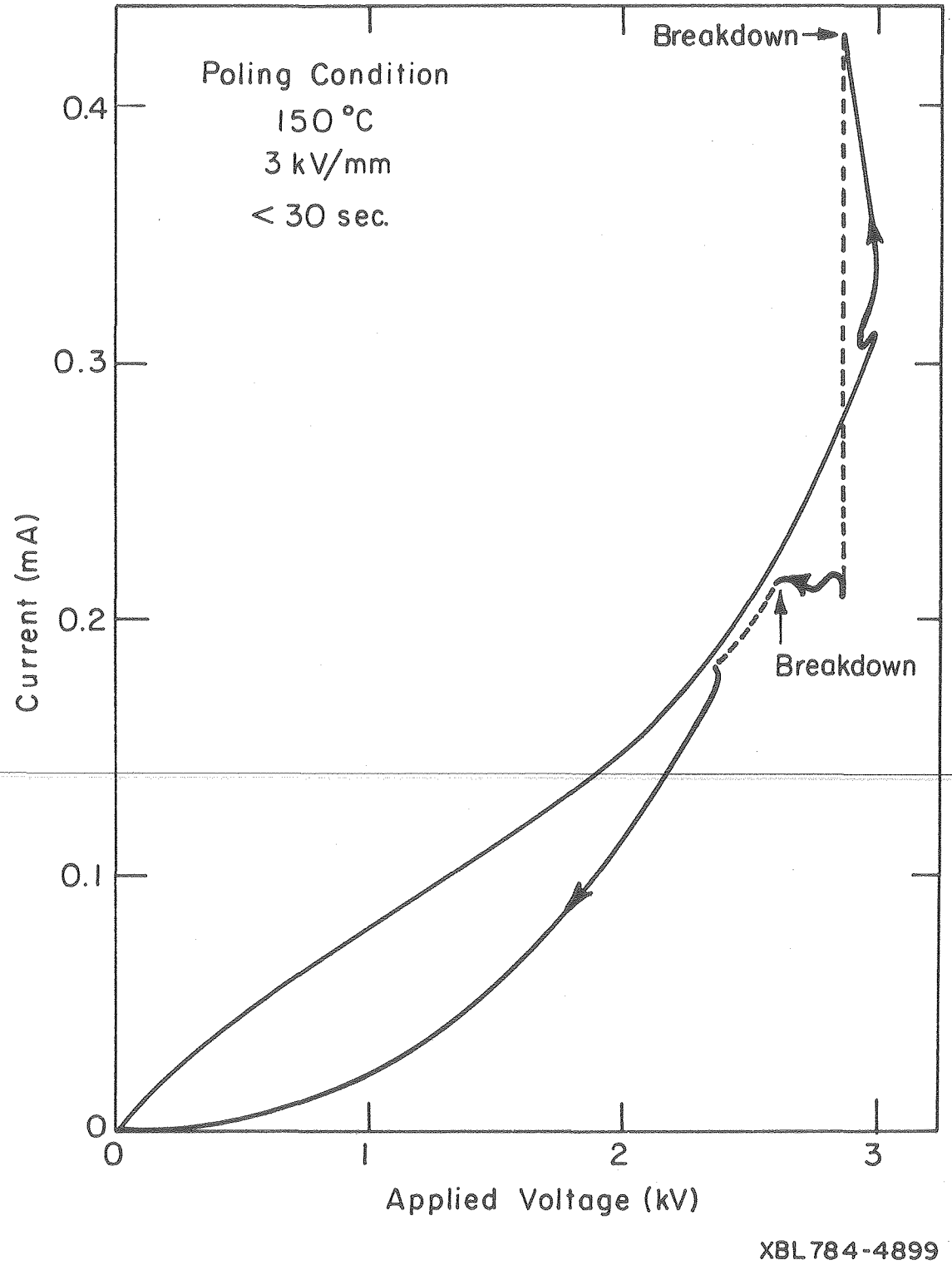
Poling Condition
150 °C
3 kV/mm
< 30 sec.
Breakdown
Breakdown
Current (mA)
0.4
0.3
0.2
0.1
0
0
1
2
3
Applied Voltage (kV)
XBL784-4899

Fig. 19

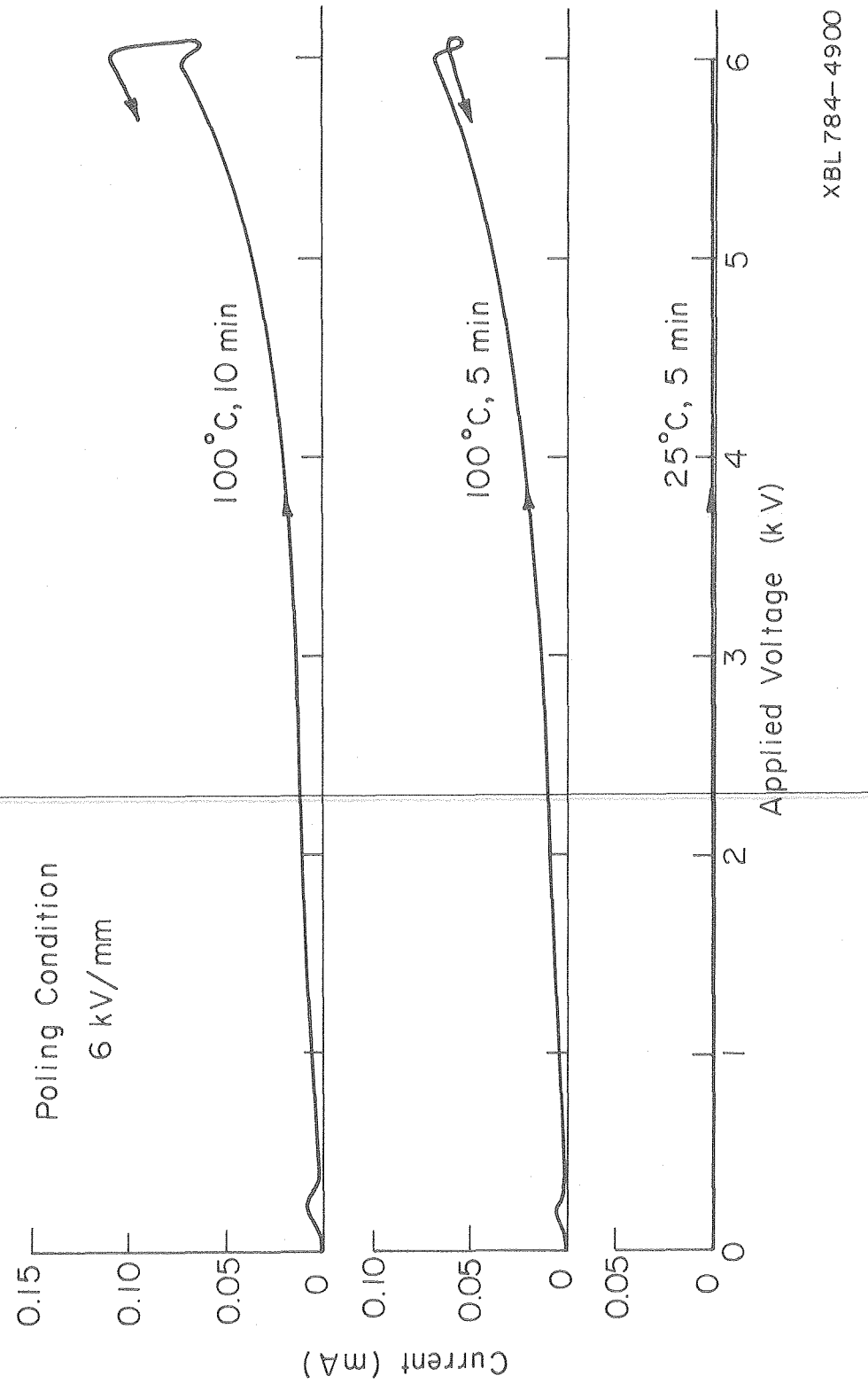

XBL 784-4900

Fig. 20

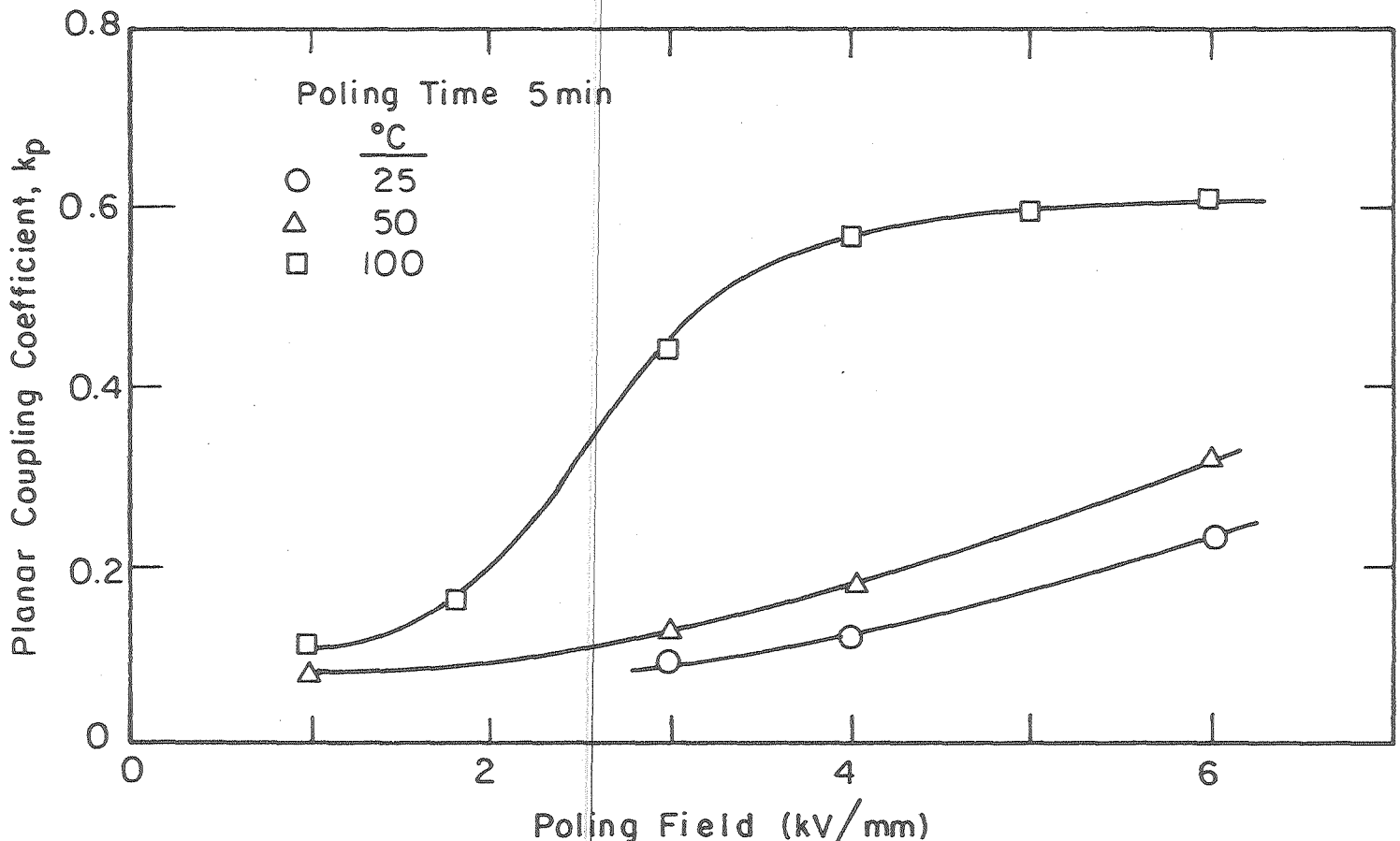

XBL784-4888

Fig. 21

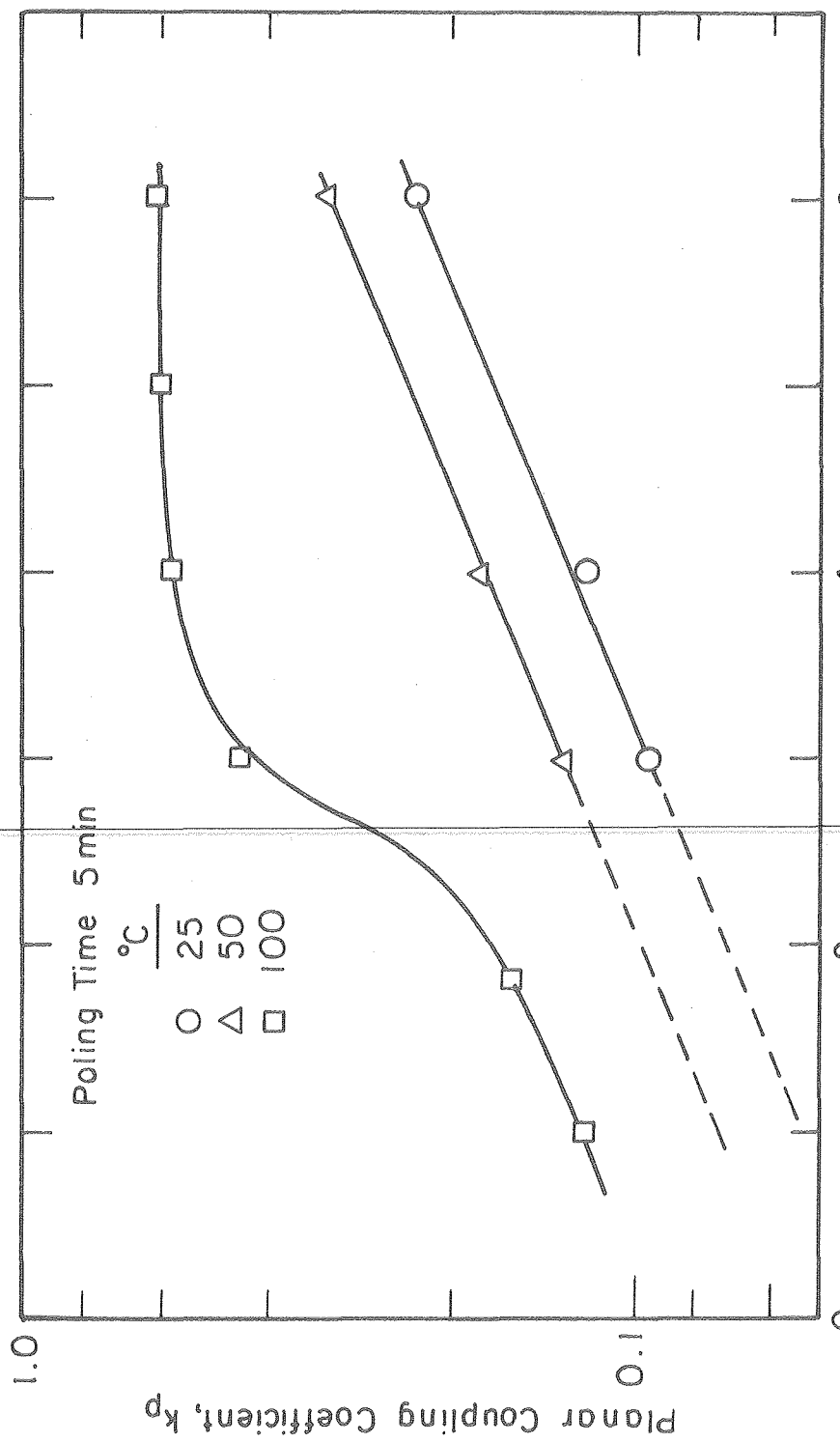

XBL 784-4890

Fig. 22

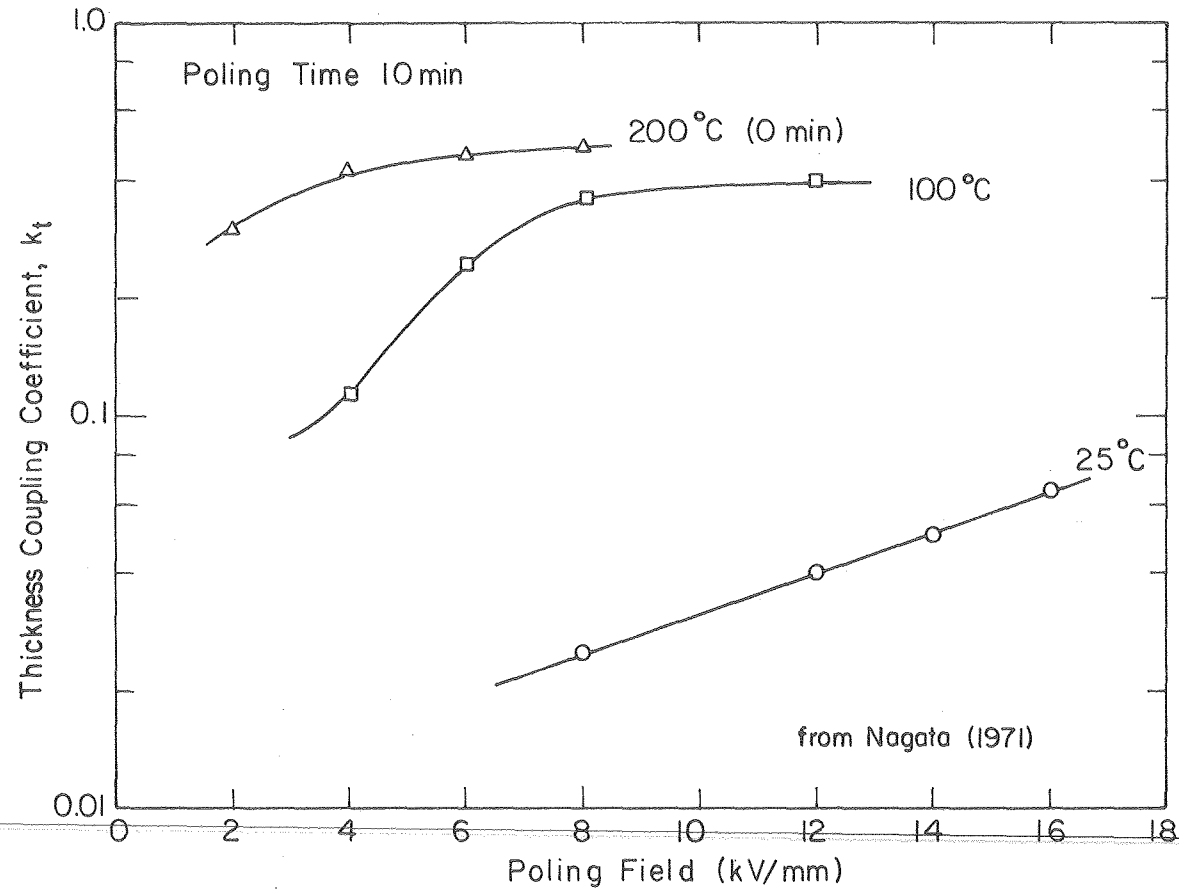

XBL784-4889

Fig. 23

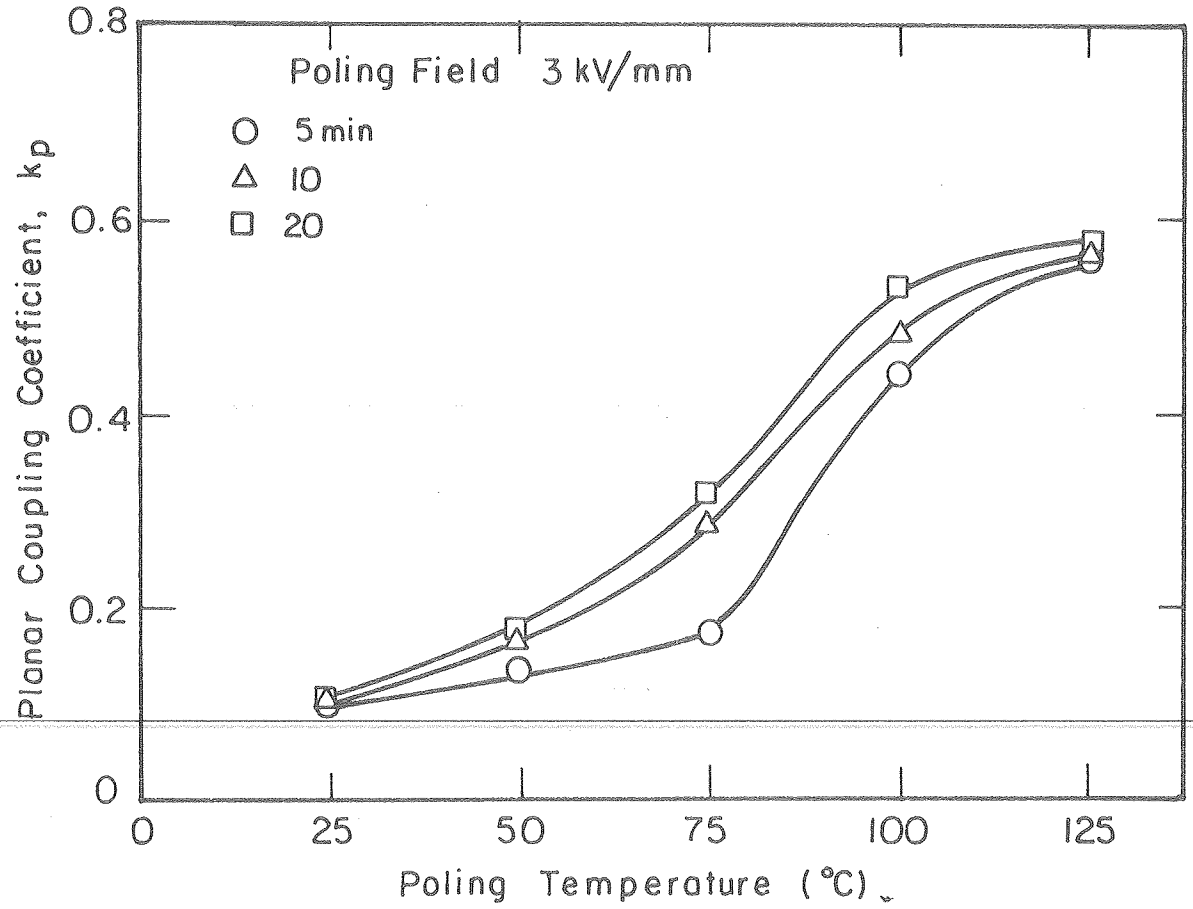
Poling Field 3 kV/mm
5 min
10
20
Planar Coupling Coefficient, kp
0.8
0.6
0.4
0.2
0
0
25
50
75
100
125
Poling Temperature (°C)
XBL 784-4884

Fig. 24

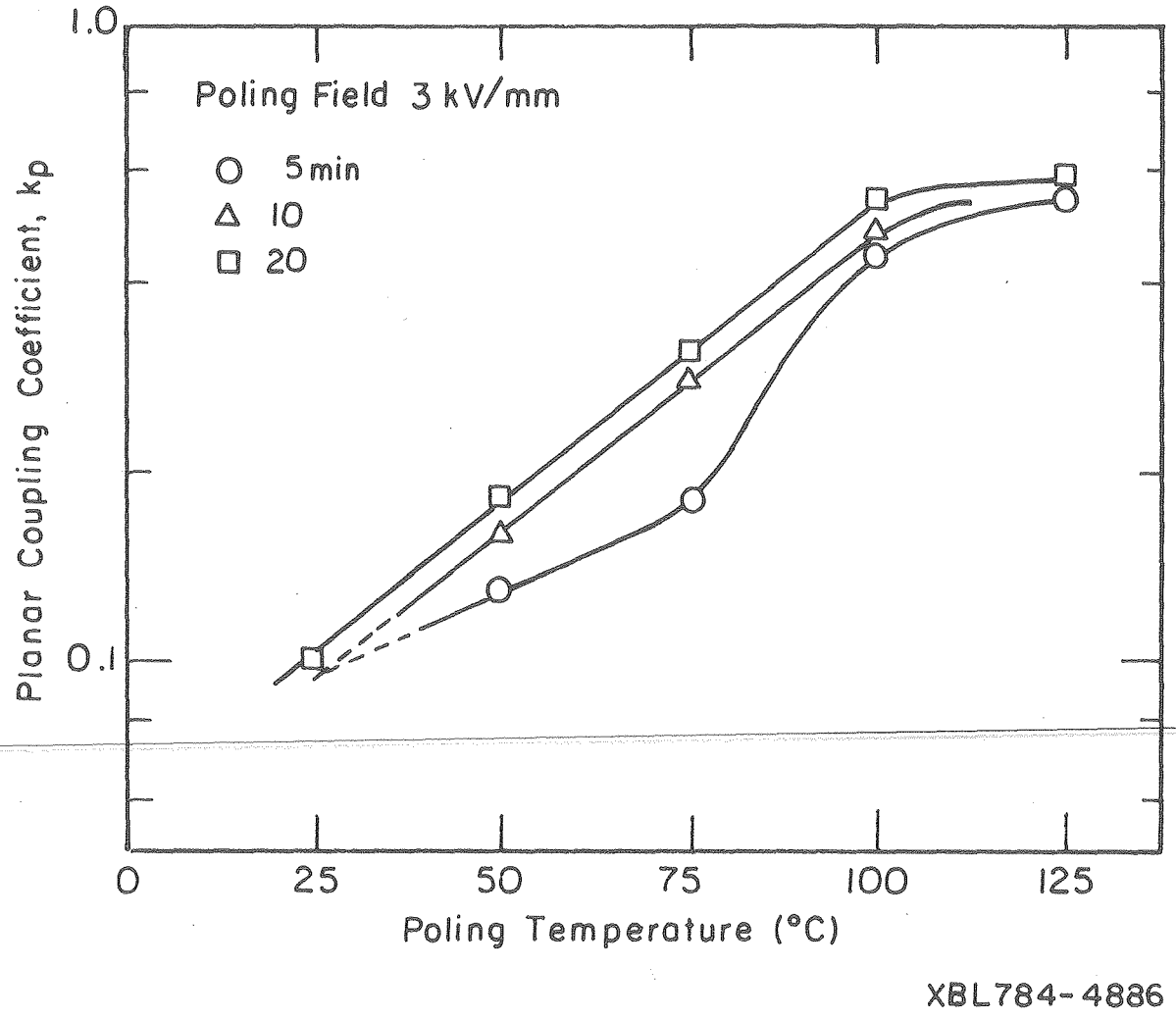
1.0
0.1
Poling Field 3 kV/mm
5 min
10
20
Planar Coupling Coefficient, kp
0
25
50
75
100
125
Poling Temperature (°C)
XBL784-4886

Fig. 25

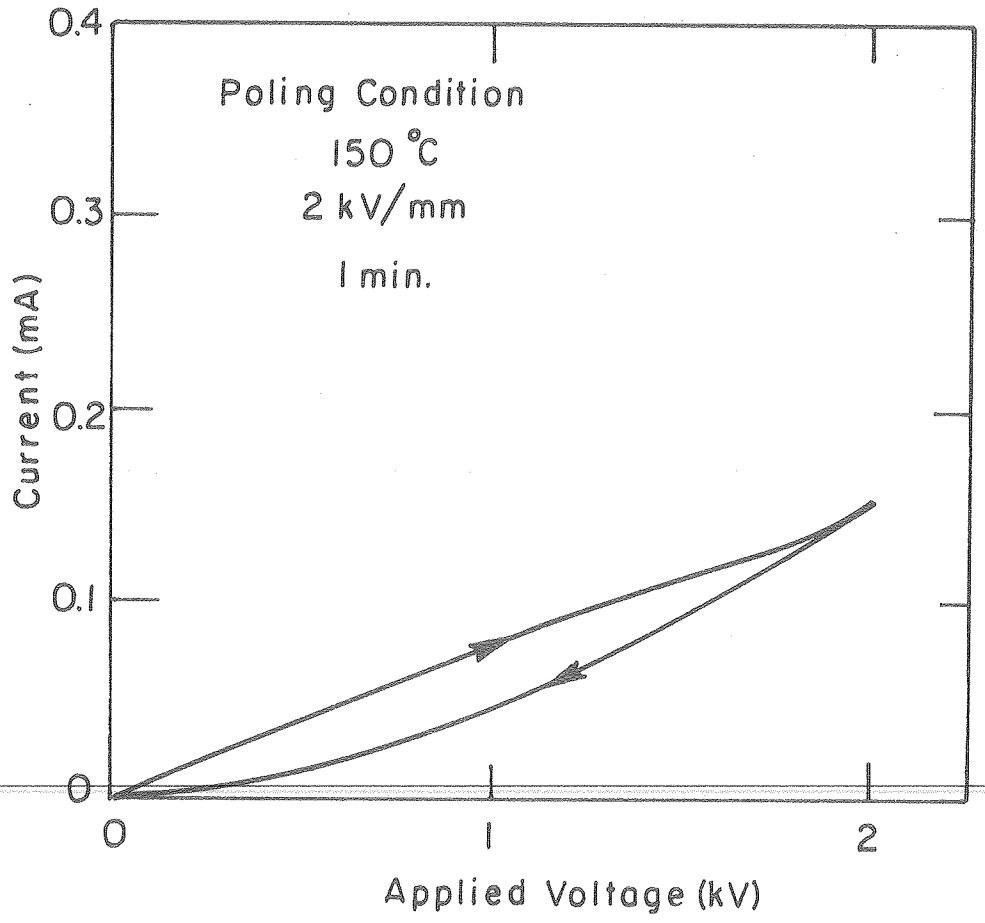

XBL 784-4898

Fig. 26

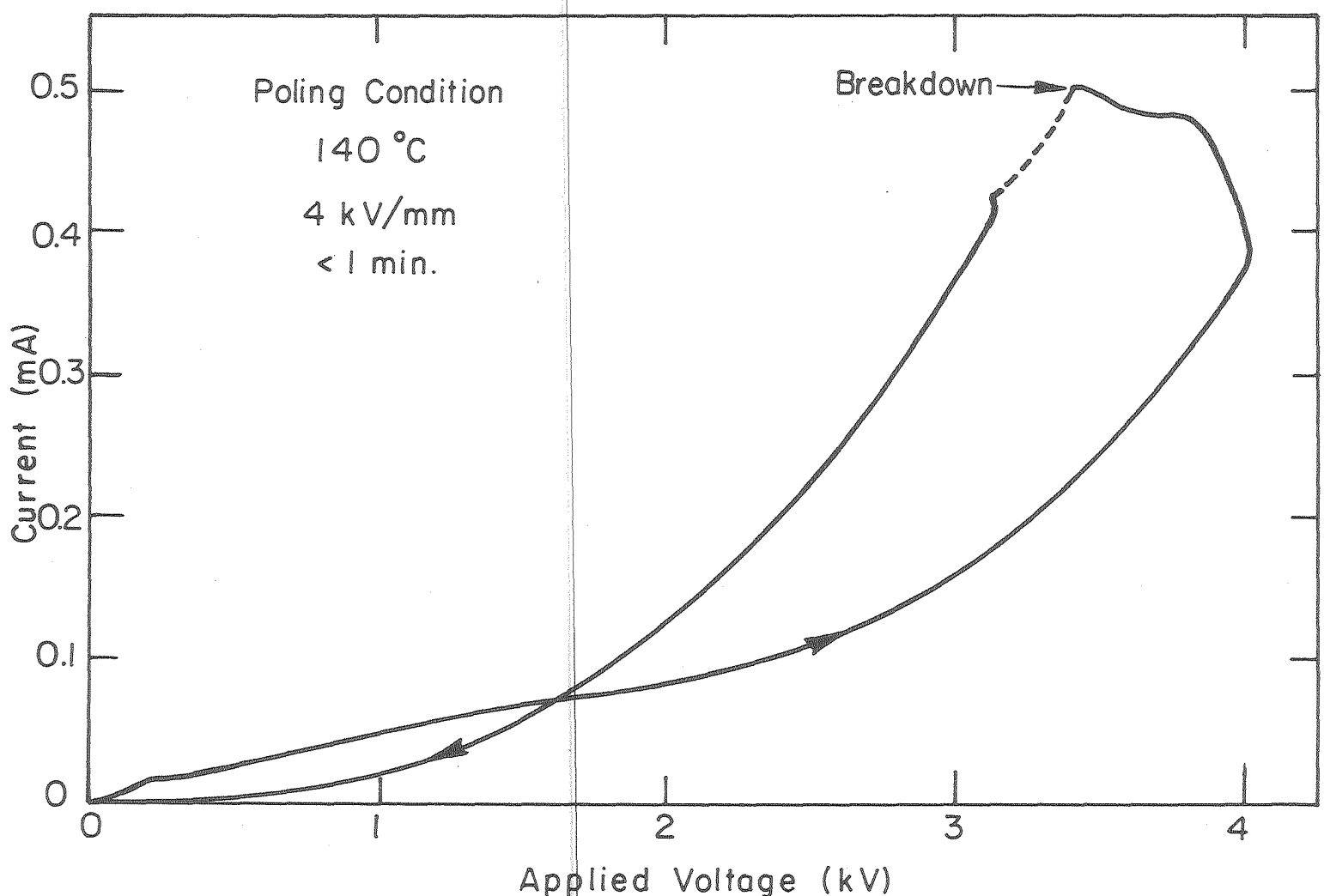

XBL784-4895

Fig. 27

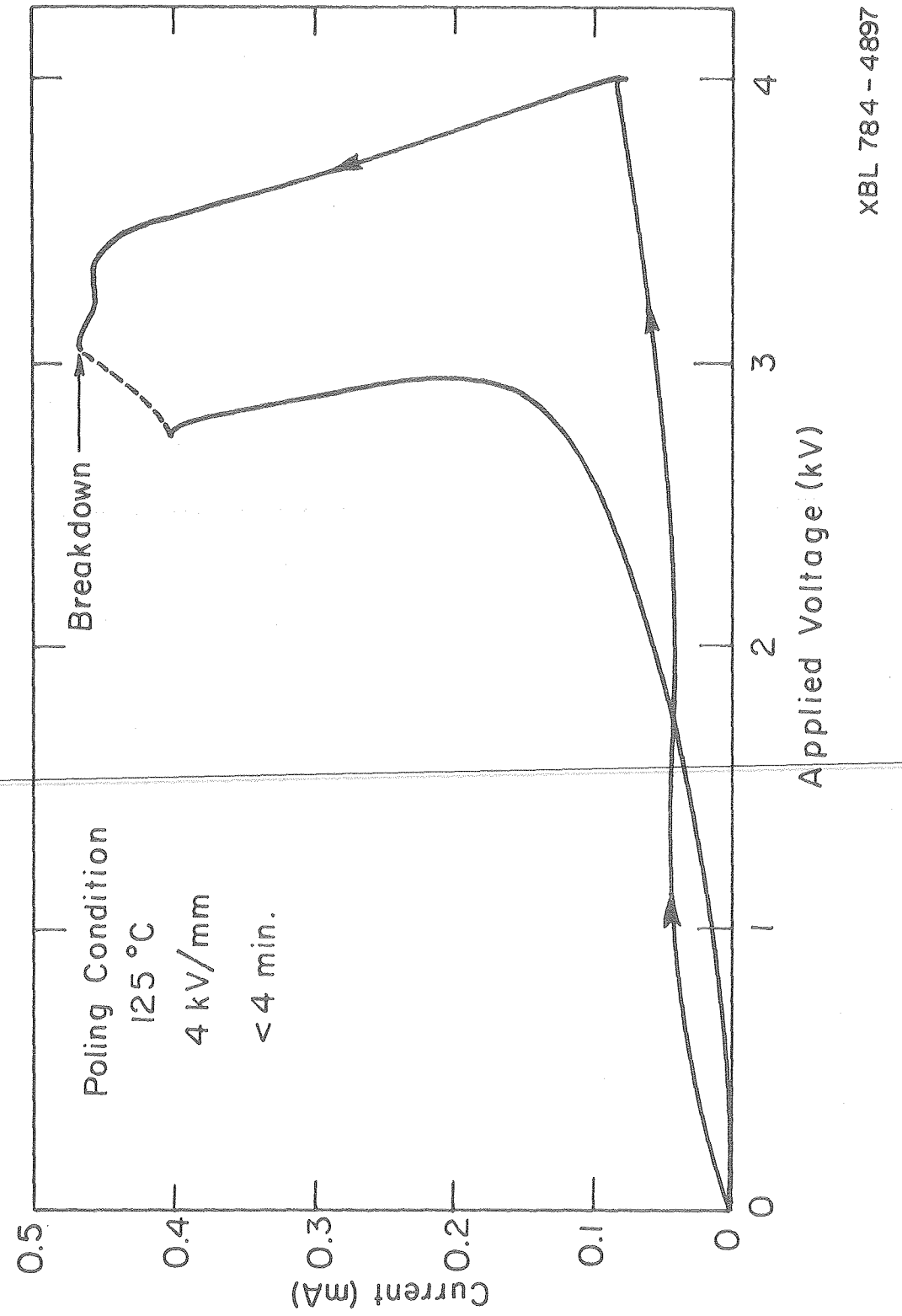

XBL 784-4897

Fig. 28

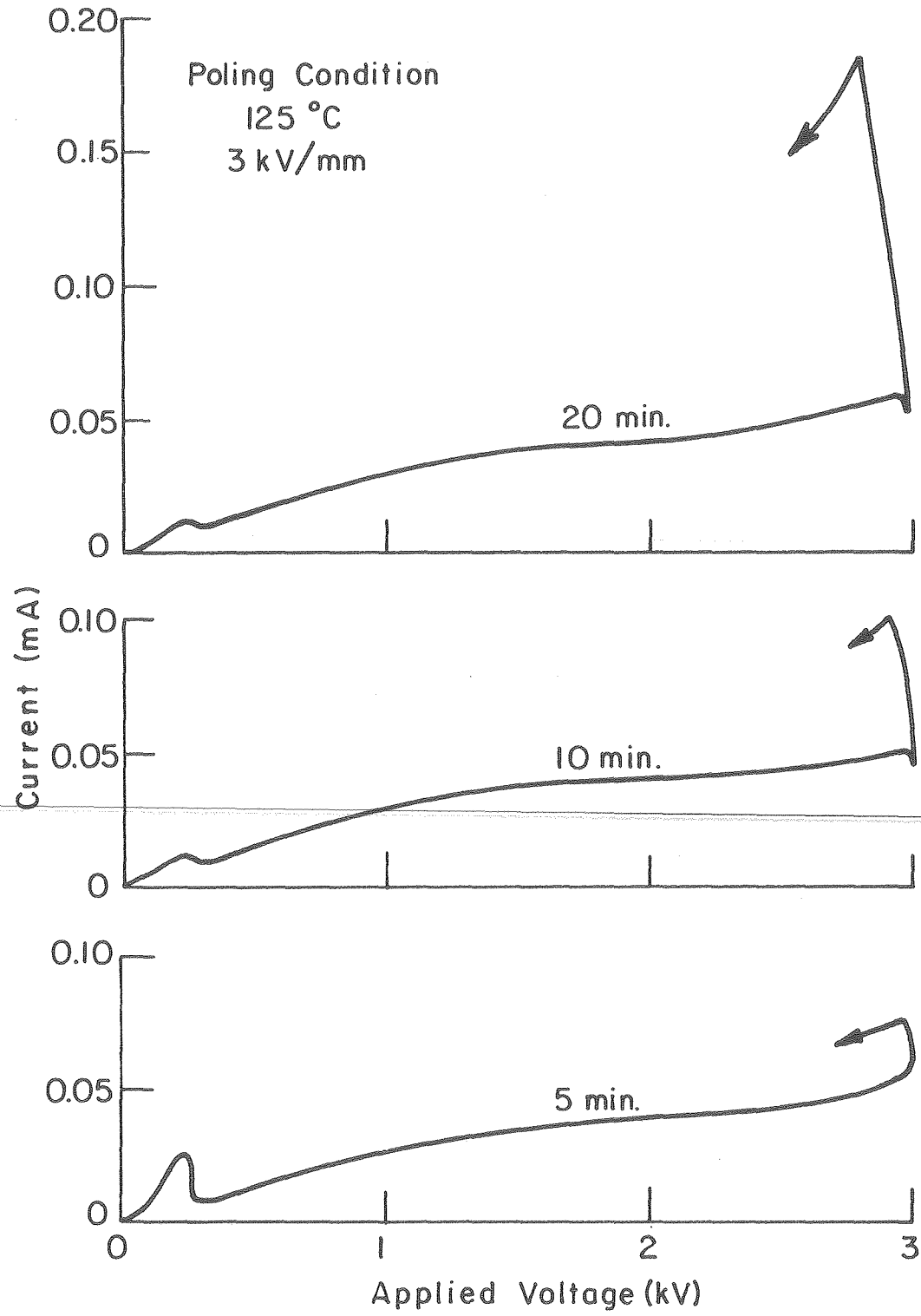
Poling Condition
125 °C
3 kV/mm
20 min.
10 min.
5 min.
Current (mA)
0.20
0.15
0.10
0.05
0
0.10
0.05
0
0.10
0.05
0
0
1
2
3
Applied Voltage (kV)
XBL784-4896

Fig. 29

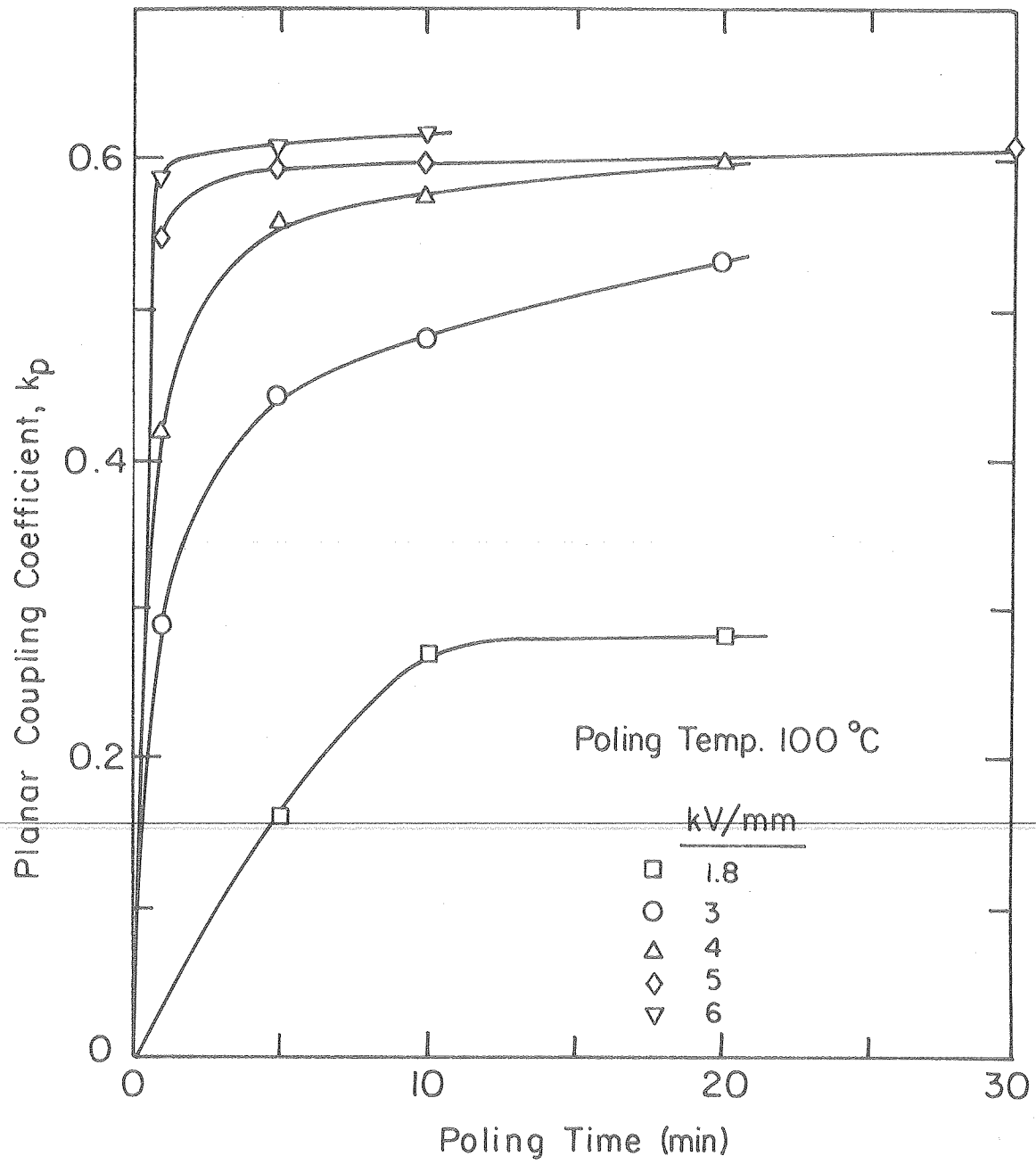
Planar Coupling Coefficient, k_p
0.6
0.4
0.2
0
0
10
20
30
Poling Time (min)
Poling Temp. 100 °C
kV/mm
1.8
3
4
5
6
XBL 784-4885

Fig. 30

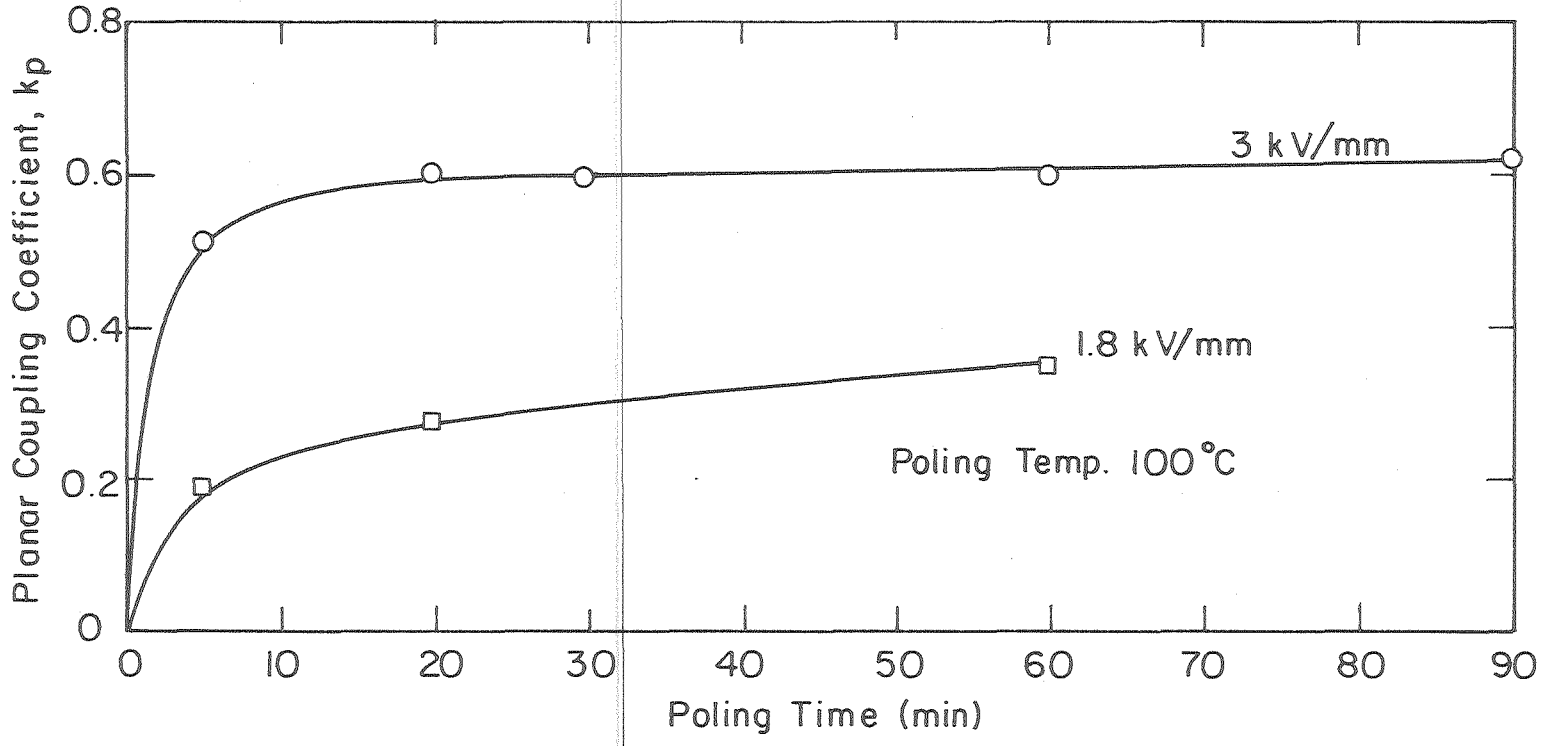

XBL 784-4887

Fig. 31

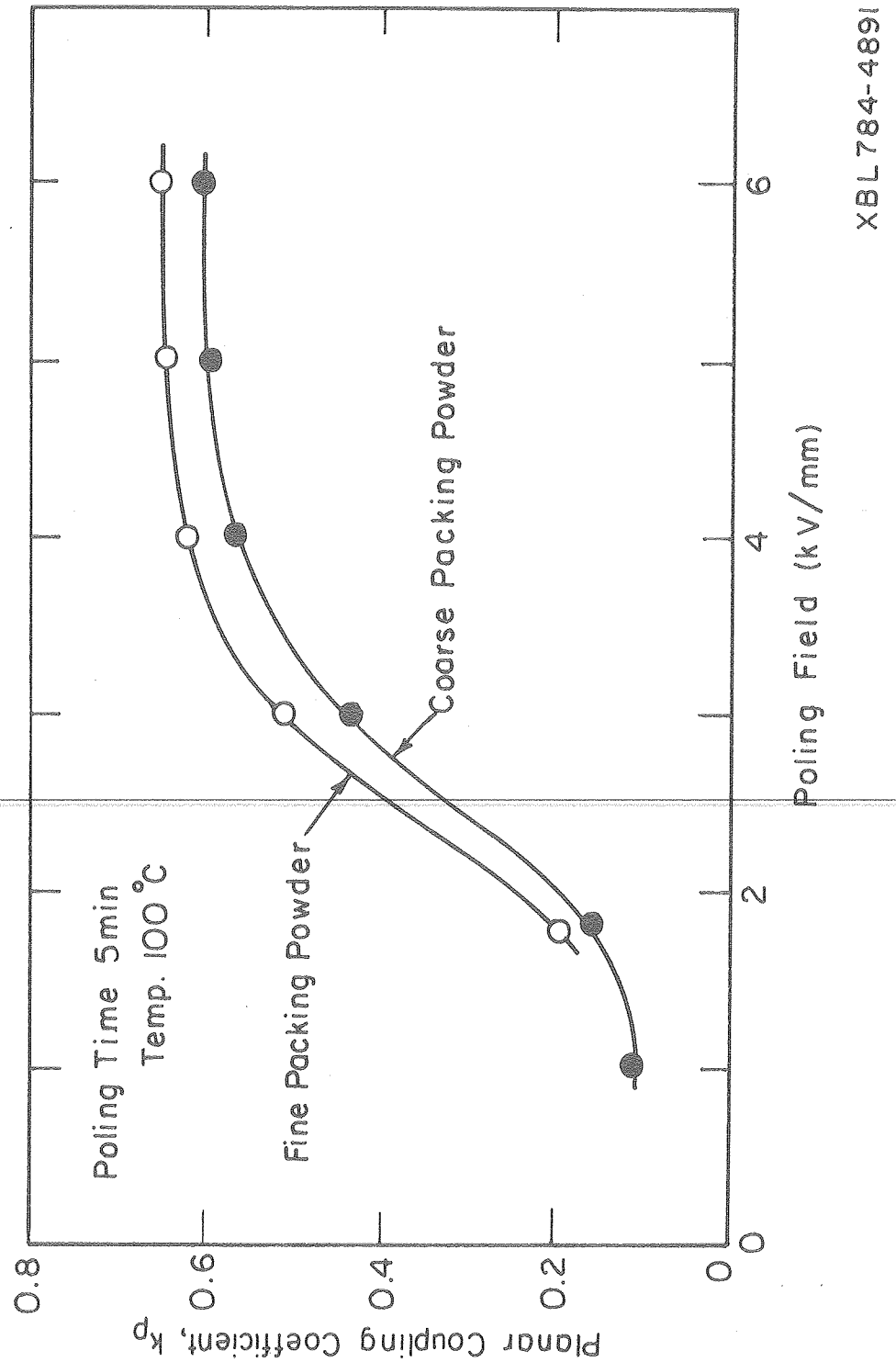
Planar Coupling Coefficient, k_p
0.8
0.6
0.4
0.2
0
0
2
4
6
Poling Field (kV/mm)
Poling Time 5min
Temp. 100°C
Fine Packing Powder
Coarse Packing Powder
XBL784-4891

Fig. 32

REFERENCES

1. B. Jaffe, R. Cook and H. Jaffe, Piezoelectric Ceramics, (Academic Press, NY, 1971).

2. J. van Randeraat and R. E. Setterington (ed.) "Piezoelectric Ceramics," (Mulliard, Ltd., London), 1974.

3. R. B. Atkin, R. L. Holman and R. M. Fulrath, "Substitution of Bi and Nb Ions in Lead Zirconate Titanate," J. Amer. Ceram. Soc., 54, (2) 113 (1972).

4. J. J. Dih and R. M. Fulrath, "Sintering of Sc Modified Lead Zirconate Titanate," J. Amer. Ceram. Soc., 60, (1-2) 92 (1977).

5. Frank Kulscar, "Electromechanical Properties of Lead Zirconate Titanate Ceramics with Lead Partially Replaced by Calcium or Strontium," J. Amer. Ceram. Soc., 42, (1) 49 (1959).

6. Final Report. Channel Product Inc., "Study of Lead Zirconate Titanate Double Additives Systems from the U.S. Patent Literature," Contract N00024-75-C-6181, Department of the Navy, Feb. 1977.

7. Robert Gerson, "Variation in Ferroelectric Characteristics of Lead Zirconate Titanate Ceramics Due to Minor Chemical Modifications," J. Amer. Ceram. Soc., 31 (1) 188, 1960.

8. G. H. Haertling and C. E. Land, "Hot-Pressed $(Pb,La)(Zr,Ti)O_3$ Ferroelectric Ceramics for Electro-optical Applications," J. Amer. Ceram. Soc., 54 (1) 1, 1971.

9. D. A. Berlincourt, C. Cmolik and H. Jaffe, "Piezoelectric Properties of Polycrystalline Lead Titanate Zirconate Compositions," Proc. IRE 48 (2) 220 (1960).

10. Sadayuki Takahashi and Masao Takahashi, "Effects of Impurities on The Mechanical Quality Factor of Lead Zirconate Titanate Ceramics," Jap. J. Appl. Phys., 11 (1) 31, 1972.

11. T. B. Weston, A. H. Webster and V. M. McNamara, "Lead Zirconate-Lead Titanate Piezoelectric Ceramics with Iron Oxide Additions," J. Amer. Ceram. Soc., 52 (5) 253 (1969).

12. Masao Takahashi, "Space Charge Effect in Lead Zirconate Titanate Ceramics Caused by the Addition of Impurities," Jap. J. Appl. Phys. 9, (10) 1236, 1970.

13. D. A. Berlincourt, D. R. Curran and H. Jaffe, "Piezoelectric and Piezomagnetic Materials and Their Function in Transducers," in Physical Acoustics (W. P. Mason, ed.) V. 1, Part A, pp 169-270 (Academic Press, NY, 1974).

14. John F. Dullea, Jr., "Variations in the Ferroelectric and Piezoelectric Properties of Lead Zirconate Titanate Ceramics Containing Cr_2O_3 Additions," M.S. Thesis, University of California at Berkeley, (1976) LBL-4551.

15. R. L. Moon, "High Temperature Phase Equilibria in the Lead Titanate-Lead Zirconate System," Ph.D. Thesis, University of California at Berkeley, (1967) UCRL-17545.

16. R. B. Atkin and Richard M. Fulrath, "Point Defects and Sintering of Lead Zirconate-Titanate," J. Amer. Ceram. Soc., 54 (5) 265 (1971).

17. Robert L. Holman and Richard M. Fulrath, "Intrinsic Nonstoichiometry in the Lead Zirconate-Lead Titanate System Determined by Knudsen Effusion," J. Appl. Phys. 44 (12) 5227 (1973).

18. David N. Northrop, "Vaporization of Lead Zirconate Titanate Materials," I and II. J. Amer. Ceram. Soc., 50 (9) 441 (1967); 51 (7) 357 (1968).

19. John W. Sherohman, Jr., "A Liquid Phase Densification Technique for the Lead Zirconate-Titanate System," Ph.D. Thesis, University of California at Berkeley (1974) LBL-2767.

20. Kenneth E. Crabtree, "Densification and Electric Properties of Controlled Stoichiometry PZT," M.S. Thesis, University of California at Berkeley (1974) LBL-3543.

21. G. H. Haertling, "Hot-Pressed Lead Zirconate-Lead Titanate Ceramics Containing Bismuth," Am. Ceram. Soc. Bull., 43 (12) 875 (1964).

22. K. Okazaki and K. Nagata, "Effects of Grain Size and Porosity in Electric and Optical Properties of PLZT Ceramics," J. Amer. Ceram. Soc., 56 (2) 82 (1973).

23. G. S. Snow, "Fabrication of Transparent Electro-optical PLZT Ceramics by Atmosphere Sintering," J. Amer. Ceram. Soc., 56 (2) 91 (1973).

24. R. B. Gray, U.S. Patent 2,486,560, Nov. 1, 1949. Filed Sept. 20, 1946.

25. S. Roberts, "Dielectric and Piezoelectric Properties of Barium Titanate," Phys. Rev., 71 (12) 890 (1947).

26. N. Bar-Chaim, N. Brunstein, J. Grunbert and A. Seidman, "Electric Field Dependence of the Dielectric Constant of PZT Ferroelectric Ceramics," J. Appl. Phys., 45 (6) pp. 2398 (1974).

27. N. Bar-Chaim, M. Brunstein, J. Grunberg and A. Seidman, "Variation of the Dielectric Constant of PZT Ferroelectric Ceramics with Electric Field," Ferroelectrics, 6 299 (1974).

28. H. Thomann, "Stabilization Effects in Piezoelectric Lead-Titanate Zirconate Ceramics," Ferroelectrics, 4 141 (1972).

29. N. Uchida and T. Ikeda, "Temperature and Bias Characteristics of $Pb(Zr, Ti)O_3$ Families Ceramics," Jap. J. Appl. Phys., 4 (11) 867 (1965).

30. H. Banno and T. Tsunooka, "Piezoelectric Properties and Temperature Dependences of Resonant Frequency of WO_3-MnO_2 Modified Ceramics of $Pb(Zr-Ti)O_3$," Jap. J. Appl. Phys., 6 (8) 954 (1967).

31. N. Uchida and T. Ikeda, "Electrostriction in Perovskite Type Ferroelectric Ceramics," Jap. J. Appl. Phys., 6 (9) 1079 (1967).

32. W. Wersing, "On the Stabilizing Field of Lead-Titanate Zirconate Ceramics Doped with Transcient Metal Ions," Ferroelectrics, 12 143 (1976).

33. Helmut Krueger, "Dispersion Study of Domain Wall Mobility and Mechanical Damping in $Pb(Zr,Ti)O_3$ Transducer Ceramics," Final Technical Report. Contract N00014-69-C-0046, Project No. NR039-100/8-26-68, Clevite Corporation, Jan. 1971.

34. Don Berlincourt and Helmut H. A. Krueger, "Domain Processes in Lead Titanate Zirconate and Barium Titanate Ceramics," J. Appl. Phys. 30 (1) 1804 (1959).

35. "Properties of Piezoelectric Ceramics," CRC Handbook of Materials Science, Vol. III, pp. 199 (CRC Press, Cleveland, OH 1975).

36. A. H. Webster, R. C. MacDonald and W. S. Bowman, J. Amer. Ceram. Soc. 34 97 (1965). Also appeared in Ref. 1, pp. 146.

37. B. Jaffe, R. S. Roth and S. Marzullo, "Properties of Piezoelectric Ceramics in the Solid Solution Series Lead Titanate - Lead Zirconate - Lead Oxide: Tin Oxide and Lead Titanate - Lead Hafnate," J. Res. Nat. Bur. Stds., 55 (5) 239 (1955).

38. S. Ikegami, I. Veda and T. Nagata, "Electrochemical Properties of $PbTiO_3$ Ceramics Containing La and Mn," J. Acous. Soc. Amer., 50 (4) 1060 (1971).

39. M. Takahashi, S. Takahashi, T. Onoe and N. Tsubouchi, "Breakdown of Lead Zirconate Titanate Ceramics Caused by the Application of Electric Field," J. Jap. Soc. Powder and Powder Met. 20 268 (1974).

40. E. Sawaguchi, J. Phys. Soc. Japan, 8 615 (1953).
G. Shirane and K. Suzuki, J. Phys. Soc. Japan, 7, 333 (1952). Also appeared in Ref. 1, pp. 136.

41. R. L. Fullman, "Measurement of Particle Size in Opaque Bodies," Trans. AIME, 197 (3) 447 (1953).

42. "IRE Standards on Piezoelectric Crystals: Measurement of Piezoelectric Ceramics, 1961," Proc. IRE, 49 1161 (1961).

43. M. Onoe, H. F. Tiersten and A. H. Meitzler, J. IECE Japan, 46 (3) 330 (1963).
Also appeared in:
K. Okazaki and H. Igarashi, "Importance of Microstructure in Electronic Ceramics," Ceramic Microstructures '76 (R.M. Fulrath and J. A. Pask, Ed.) Westview Press, Boulder, CO (1977).

45. W. R. Bratschun, "An Unusual Dielectric Failure of a Piezoelectric Ceramic," J. Appl. Phys. 36 (8) 2589 (1965).

46. P. Schnabel, "Dispersion of Thickness Vibration of Piezoelectric Disk Resonators," IEEE TRans. Son. Ultrason, SU-25 (1) 16, (1978).

This report was done with support from the Department of Energy. Any conclusions or opinions expressed in this report represent solely those of the author(s) and not necessarily those of The Regents of the University of California, the Lawrence Berkeley Laboratory or the Department of Energy.

TECHNICAL INFORMATION DEPARTMENT
LAWRENCE BERKELEY LABORATORY
UNIVERSITY OF CALIFORNIA
BERKELEY, CALIFORNIA 94720